where k_L is the (variable) incoming lab momentum, and k_{L1} and k_{L2} are the momenta of Refs. 1 and 2, respectively.[11] Then we have

$$R_1(\rho)=\frac{L(\rho,k_L)}{L(\rho,k_{L1})}\frac{k^2_{L1}}{k^2_L},\quad R_2(f^0)=\frac{I(f^0,k_L)}{I(f^0,k_{L2})}\frac{k^2_{L2}}{k^2_L}\text{ etc.}$$

The ratios R_1 and R_2 are shown in Figs. 5 and 6. We see that ρ production in experiments of type (1) is strongest below $k_L=3$ BeV/c, while f^0 production reaches its maximum there. In experiments of type (2), on the other hand, the situation is reversed: f^0 production is stronger above $k_L=3$ BeV/c, while ρ production is at its maximum there, so that, as we saw in 2(b), it is advantageous to do the experiment in the region of 4 BeV/c. As far as magnitudes are concerned, the cross sections given in Refs. 1 and 2 are, approximately,

$$\frac{\partial\sigma}{\partial m}(\rho,k_{L1})=0.52\text{ mb/50 MeV},$$

$$\frac{\partial\sigma}{\partial m}(f^0,k_{L1})=0.23\text{ mb/50 MeV},$$

$$\frac{\partial\sigma}{\partial m}(\rho,k_{L2})=0.2\text{ mb/10 MeV},$$

$$\frac{\partial\sigma}{\partial m}(f^0,k_{L2})=0.14\text{ mb/10 MeV},$$

where no correction for background has been made, and where the fourth number is based on the estimate of 1(a).

[11] R_1 and R_2 refer to reactions (1) and (2), respectively.

ACKNOWLEDGMENTS

I am grateful to Professor S. D. Drell for suggesting this calculation, to Professor J. Steinberger for several conversations about this experiment, to Dr. M. M. Sternheim for help with the programming, and to Professor G. C. Wick for his interest and encouragement.

PHYSICAL REVIEW VOLUME 131, NUMBER 4 15 AUGUST 1963

Low-Energy Intranuclear Cascade Calculation*

HUGO W. BERTINI

Oak Ridge National Laboratory,† Oak Ridge, Tennessee

(Received 19 September 1962; revised manuscript received 19 April 1963)

Monte Carlo cascade calculations have been performed for nuclear reactions involving incident protons, neutrons, π^+, and π^- on complex nuclei. The upper energy limit of validity of the calculation is $\approx$350 MeV below which pion production is not likely. In order to determine the effects of a diffuse nuclear edge, calculations were performed both for nucleon-density distributions within the nucleus which approximated the charge distribution obtained from electron-scattering data and for constant-density distributions. The results indicate that the bulk of the effect in going from a uniform to nonuniform nucleon-density distribution is due to the increased nuclear size when a diffuse edge is used, while the effects due to the diffuse edge alone are of second order. The limits of application of the general model have been investigated and are discussed.

INTRODUCTION

THE basic assumption in calculations of intranuclear cascades is that nuclear reactions involving incident particles of high energy can be described in terms of particle-particle collisions within the nucleus. The justification for this assumption is that the wavelength of the incoming particle and subsequent collision products is of the order of or smaller than the average internucleon distance within the nucleus ($\approx 10^{-13}$ cm). On the basis of this assumption, one can calculate the reaction with the nucleus by determining the life history of every particle that becomes involved in the individual particle-particle collisions occurring within the nucleus. The point of collision, the type of collision, the momentum of the struck nucleon, and the scattering angles for each collision are determined by statistical sampling techniques. Free-particle experimental data are used whenever cross-section data are required. The basic approach was suggested by Serber,[1] and statistical calculations based on his suggestion were first reported by Goldberger.[2] The latest and most complete calculation of this type was that of Metropolis *et al.*[3,4]

Some of the major features of the nuclear model used by Metropolis *et al.* are that the nucleon density within the nucleus was assumed to be a constant; a zero-

* Submitted to the University of Tennessee in partial fulfillment of the degree of Doctor of Philosophy.

† Operated by Union Carbide Corporation for the U. S. Atomic Energy Commission.

[1] R. Serber, Phys. Rev. **72**, 1114 (1947).

[2] M. L. Goldberger, Phys. Rev. **74**, 1268 (1948).

[3] N. Metropolis, R. Bivins, M. Storm, Anthony Turkevich, J. M. Miller, and G. Friedlander, Phys. Rev. **110**, 185 (1958).

[4] N. Metropolis, R. Bivins, M. Storm, J. M. Miller, G. Friedlander, and Anthony Turkevich, Phys. Rev. **110**, 204 (1958).

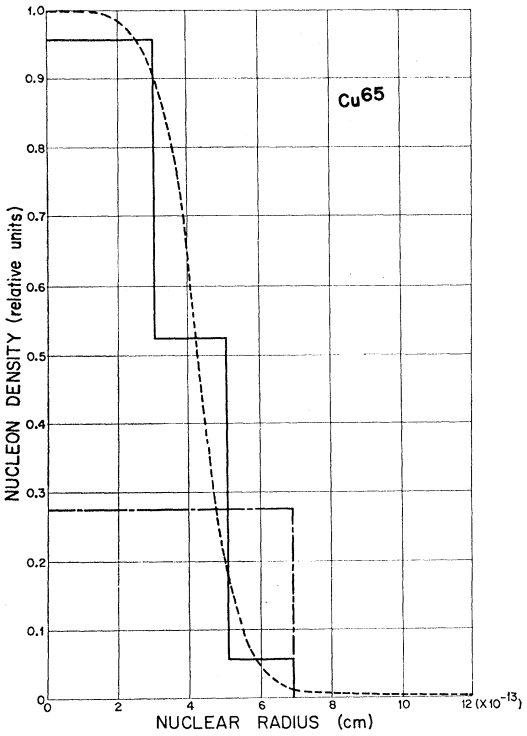

FIG. 1. A comparison of various nucleon-density distributions for nucleons inside the nucleus. Solid line, standard three-region configuration; long-dash—short-dash line, uniform distribution; dashed line, Hofstadter's curve (see Ref. 5).

temperature Fermi-energy distribution was used to represent the energy distribution of the nucleons inside the nucleus; and the potential for pions within the nucleus was assumed to be zero. The results of their work indicated that the model could be applied reasonably well to most problems; however, there were discrepancies between calculations and experiments which were usually attributed to the deficiencies in the nuclear model. The purpose of the present work is to investigate the existing discrepancies by using an improved model and to attempt to determine the areas of agreement and disagreement with experiment by a more extensive comparison with available data. The same general approach as described above is used.

NUCLEAR MODEL

The density distribution of the protons inside the nucleus was made to approximate the nonzero Fermi-type charge-distribution function obtained from electron-scattering data.[5] Three concentric spheres were used for the approximation (i.e., a central sphere and two surrounding spherical annuli). The radii of the spheres were determined by the distances at which the Fermi-type charge-distribution function reached various fractions of the central density. In the standard configuration used here, the fractions were 0.9, 0.2, and 0.01. The boundaries applied to both neutrons and protons. The proton density in each region was set equal to the average value of the charge distribution in that region. The neutron-to-proton density ratio in each region was the same and was equal to the ratio of neutrons to protons in the nucleus. Neutron or proton deficiencies at the nuclear surface over and above this ratio are not clearly established, but they appear to be small[6] and would be completely masked in the present calculation. A uniform or constant density distribution was obtained by setting the two inner radii equal to the outer radius. An example of these configurations is given in Fig. 1. When nonstandard configurations are used they will be noted.

In each region the neutrons and protons were assumed to have a zero-temperature Fermi-energy distribution where the zero-temperature Fermi energies were determined by the nucleon densities. The composite momentum distribution for the entire nucleus is not a zero-temperature Fermi distribution, but is a distribution which can be roughly approximated by a Gaussian with a kT value of 15 MeV. This is in the range of values for the Gaussian distributions which are

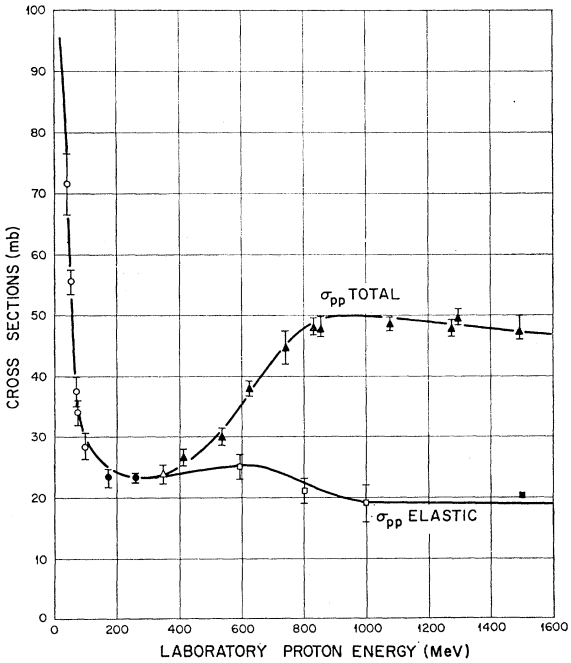

FIG. 2. Proton-proton total and elastic cross sections versus energy. ○, U. E. Kruse, J. M. Teem, and N. F. Ramsey, Phys. Rev. **101**, 1079 (1956). ●, O. Chamberlain and J. D. Garrison, Phys. Rev. **95**, 1349 (L) (1954). △, O. Chamberlain, E. Segrè, and C. Wiegand, Phys. Rev. **83**, 923 (1951). ▲, F. F. Chen, C. P. Leavitt, and A. M. Shapiro, Phys. Rev. **103**, 211 (1956). □, L. W. Smith, A. W. McReynolds, and G. Snow, Phys. Rev. **97**, 1186 (1955). ■, W. B. Fowler, R. P. Shutt, A. M. Thorndike, and W. L. Whittemore, Phys. Rev. **103**, 1479 (1956).

[5] R. Hofstadter, Rev. Mod. Phys. **28**, 214 (1956).

[6] L. Wilets, Rev. Mod. Phys. **30**, 542 (1958).

obtained from experimental data[7] and which are used to represent the nucleon momentum distributions within the nuclei.

The binding energy of the most loosely bound nucleon was assumed to be 7 MeV for all of the regions and for all of the nuclei. The potential inside the nucleus for each type of nucleon in each region was taken to be 7 MeV greater than the corresponding zero-temperature Fermi energy. The pion potential was arbitrarily assumed to be equal to the potential of the nucleon with which it was interacting; hence the same potentials were used for pions as for nucleons. This is in reasonable agreement with calculations of the pion potential which are based on experiments.[8]

As the cascade particles crossed the region boundaries, they gained or lost kinetic energy in the amount in which the potential was more negative or less negative.

The effects of refraction at the nuclear surface and clusters (other than for pion absorption) were not included in the calculation. The effects of the reduction in the average nuclear density of the bound nucleons as they became involved in the cascade was not taken into account. The cascade particles move through the nucleus with a velocity greater than the velocity with which a disturbance is likely to be propagated. Therefore, most of the time they will be passing through undisturbed nuclear matter.

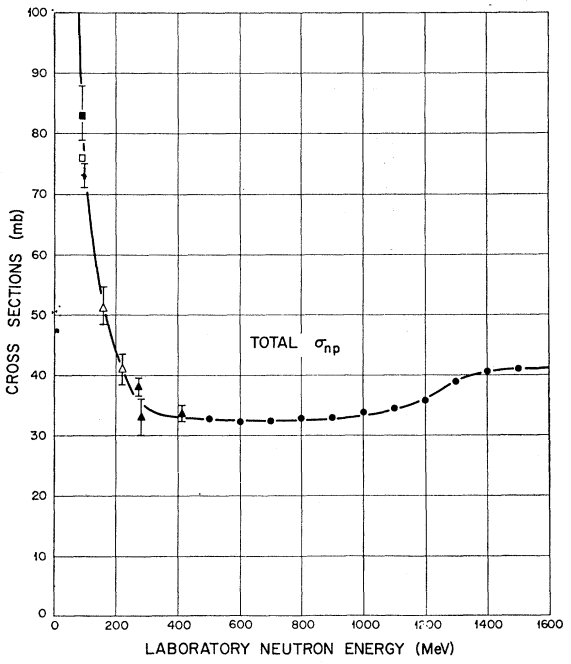

FIG. 3. Neutron-proton total cross sections versus energy. ■ L. J. Cook, E. M. McMillan, J. M. Peterson, and Duane C. Sewell, Phys. Rev. **75**, 7 (1949). □ J. Hadley, E. Kelly, C. Leith, E. Segrè, C. Wiegand, and H. York, Phys. Rev. **75**, 351 (1949). ▼ J. De Juren and N. Knable, Phys. Rev. **77**, 606 (1956). △ J. De Juren and B. J. Moyer, Phys. Rev. **81**, 919 (1951). ▲ A. V. Nedzel, Phys. Rev. **94**, 174 (1954). ● F. F. Chen, C. P. Leavitt, and A. M. Shapiro, Phys. Rev. **103**, 211 (1956).

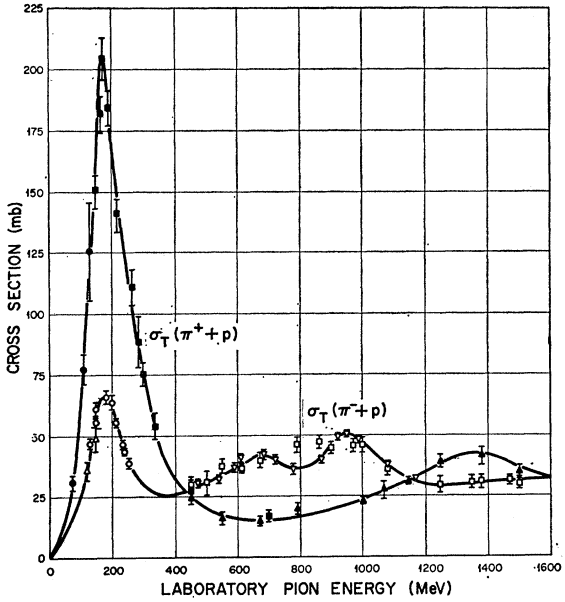

FIG. 4. π^+-proton and π^--proton total cross sections versus energy. ●, △ H. L. Anderson, E. Fermi, R. Martin, and D. E. Nagle, Phys. Rev. **91**, 155 (1953). ■ S. J. Lindenbaum and L. C. L. Yuan, Phys. Rev. **100**, 306 (1955). ▲, □ R. Cool, O. Piccioni, D. Clark, Phys. Rev. **103**, 1082 (1956). ○ J. Ashkin, J. P. Blaser, F. Feiner, J. G. Gorman, and M. O. Stern, Phys. Rev. **96**, 1104 (1954). ▽ H. C. Burrowes, D. O. Caldwell, D. H. Frisch, D. A. Hill, D. M. Ritson, R. A. Schluter, and M. A. Wahlig, Phys. Rev. Letters **2**, 119 (1959).

CROSS-SECTION DATA AND SAMPLING METHOD

The total cross sections that were used in the calculation are illustrated in Figs. 2–4. Although both total and elastic cross sections are illustrated in Fig. 2, only the total cross section was used in this work because pion production was ignored. The neutron-proton cross sections below 100 MeV were taken from the compilation of Hughes and Schwartz.[9] The proton-proton cross sections below 50 MeV were calculated from the differential cross sections given by Beretta *et al.*[10] by estimating those parts of the differential cross-section curves which were due to nuclear forces alone and then integrating over them.

The nucleon-nucleon differential cross sections were taken from the work of Hess.[11] Semiempirical fits were made to these data by using second- and third-degree

[7] L. S. Azhgirey *et al.*, Nucl. Phys. **13**, 258 (1959); J. D. Dowell *et al.*, Proc. Phys. Soc. (London) **75**, 24 (1960); J. M. Wilcox and B. M. Moyer, Phys. Rev. **99**, 875 (1955).

[8] T. A. Fujii, Phys. Rev. **113**, 695 (1959); D. H. Stork, *ibid.* **93**, 868 (1954); A. M. Shapiro, *ibid.* **84**, 1063 (1951); A. Pevsner, J. Rainwater, R. E. Williams, and S. J. Lindenbaum, *ibid.* **100**, 1419 (1955).

[9] D. J. Hughes and R. B. Schwartz, BNL-325, 1958 (unpublished).

[10] L. Beretta, C. Villi, and F. Ferrari, Nuovo Cimento **12**, S499 (1954).

[11] W. N. Hess, Rev. Mod. Phys. **30**, 368 (1958).

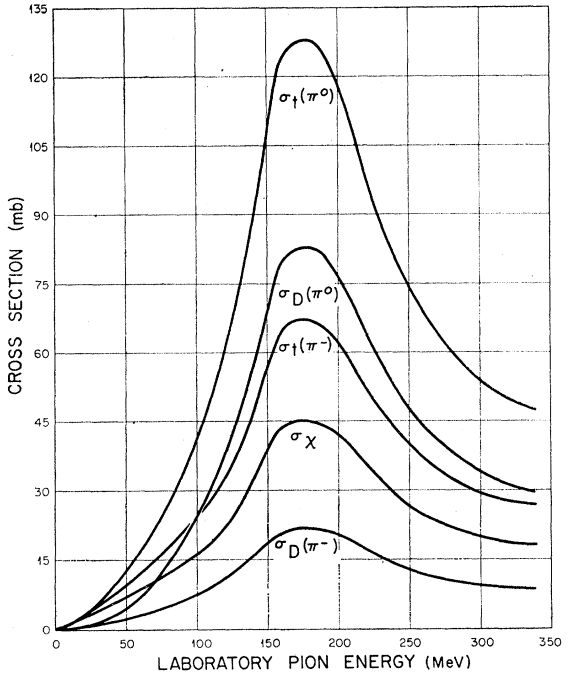

FIG. 5. Calculated pion-proton cross sections versus pion energy. $\sigma_t(\pi^0)$ Total cross section for π^0+p scattering. $\sigma_D(\pi^0)$ Cross section for π^0+p elastic scattering. $\sigma_t(\pi^-)$ Experimental π^-+p total cross section included for comparison purposes. σ_x Cross section for π^-+p, π^++n, π^0+p, and π^0+n exchange scattering. $\sigma_D(\pi^-)$ Cross section for π^-+p elastic scattering.

polynomials so that the cross section could be represented as a function of energy.

The pion-nucleon differential cross sections were calculated from the phase shifts of Orear.[12] Charge independence was assumed, and as a consequence, the differential cross sections for elastic scattering in π^-+p and π^++n reactions become equal; the same is true for π^0+p and π^0+n reactions. It also follows that the differential cross sections for charge-exchange scattering are equal. All calculated total cross sections were related to the experimental π^-+p elastic cross section, and they are illustrated in Fig. 5.

The pion-nucleon absorption cross section as computed by Metropolis *et al.* was used to determine the mean-free path for pion absorption. As in their work, pion absorption was assumed to occur via a two-nucleon cluster. However, in the present work the type of cluster was chosen with a probability that is determined by the number of each type of particle pair within the nucleus (*p-p*, *n-p*, *n-n*). Pair types which would violate charge conservation were not included in the calculation of the probabilities. To illustrate, π^+ absorption could take place with *n-p* and *n-n* pair clusters only. When a π^+ absorption occurred, the probability of the pair type being an *n-p* pair is given by the ratio of the number of *n-p* pairs to the sum of *n-p* and *n-n* pairs in the nucleus. The probability for π^+ and π^- absorption taking place with *n-p* pairs calculated in this way is consistent with the probability deduced from experiment.[13] The absorption mean-free path in the nuclear matter was assumed to be the same for the three types of pions. The cross-section data were tabulated at every 20-MeV interval.

In the sampling technique used, the point of collision, type of collision, and momentum of the struck particle are all chosen simultaneously by a rejection technique.[14] This technique is exact in the sense that it yields a distribution function $e^{-\Sigma x}\Sigma$ for the distance traveled by the particle, where Σ is the total macroscopic cross section averaged over the momentum distribution of the nucleons in the nucleus. At the same time the momentum of the struck particle is chosen from a distribution function which is the fraction of the total

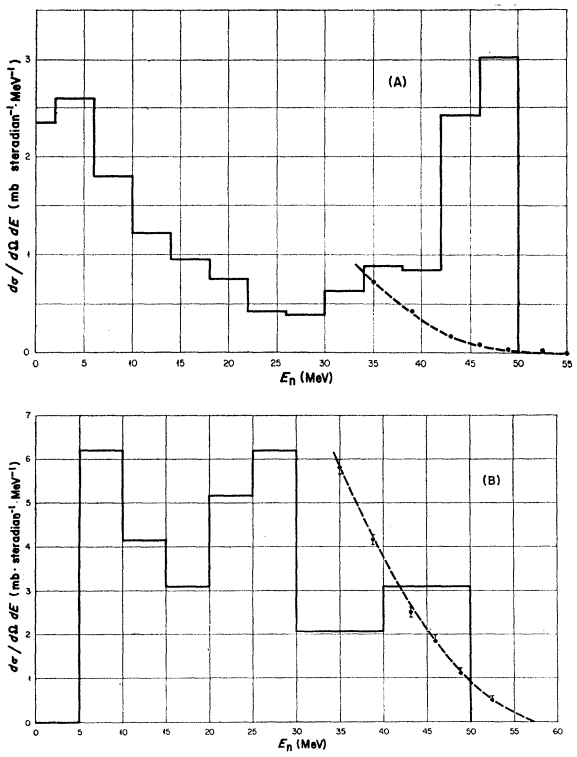

FIG. 6. Neutron spectra at 0° from 50-MeV protons on (A) C and (B) Pb. Dashed curve: Hofmann's experimental results [J. A. Hofmann, Ph. D. thesis, Harvard University, Cambridge, Massachusetts 1952 (unpublished)]; solid lines: calculated spectrum for neutrons emitted in the angular interval 0° to 10°.

[12] J. Orear, Phys. Rev. **100**, 288 (1955).

[13] S. Ozaki, R. Weinstein, G. Glass, E. Loh, L. Neimala, and A. Wattenberg, Phys. Rev. Letters **4**, 533 (1960); N. J. Petrov, V. G. Ivanov, V. A. Rusakov, Zh. Eksperim. i Teor. Fiz. **37**, 954 (1959) [translation: Soviet Phys.—JETP **10**, 682 (1960)]; G. A. Blinov, M. F. Lomanov, Ia. Ia. Shalamor, V. A. Shebanor, and V. A. Schegoler, Zh. Eksperim. i Teor. Fiz. **35**, 880 (1958) [translation: Soviet Phys.—JETP **8**, 609 (1959)]; A. Tomasini, Nuovo Cimento **3**, 160 (1956); V. DeSabbato, E. Monaresi, and G. Puppi, *ibid.* **10**, 1704 (1953).

[14] C. D. Zerby, R. B. Curtis, and H. W. Bertini, ORNL-CF-61-7-20, 1961 (unpublished).

reaction rate per unit volume taking place with nucleons whose momenta are in $d\bar{p}$ about $\bar{p}$. Relativistic effects are included in this function.

The history of each particle involved in the collision was traced until the particle either escaped or until its energy, measured with respect to the outside of the nucleus, became lower than some cutoff energy which was arbitrarily taken to be one-half the Coulomb potential at the surface of the nucleus. An attempt was made to include exclusion effects by insisting that the nucleons have energies greater than the Fermi energy after a collision. Otherwise, the initial particle was treated as though no collision had occurred. Relativistic kinematics were used for every collision.

COMPARISON WITH THE WORK OF METROPOLIS ET AL.

Graphs and tables giving direct comparisons of the present work with the work of Metropolis *et al.*[3,4] are published elsewhere.[15] For these comparisons calculations were performed for two nuclear configurations: one the same as that used by Metropolis *et al.* (i.e., having a radius given by $r=r_0A^{1/3}$ with a uniform nucleon density distribution); and the other the standard nuclear configuration described previously. The first configuration is referred to as a small (radius), uniform (nucleon density distribution) configuration. The following paragraphs summarize the results of the comparisons. For more details, the reader must refer to Ref. 15.

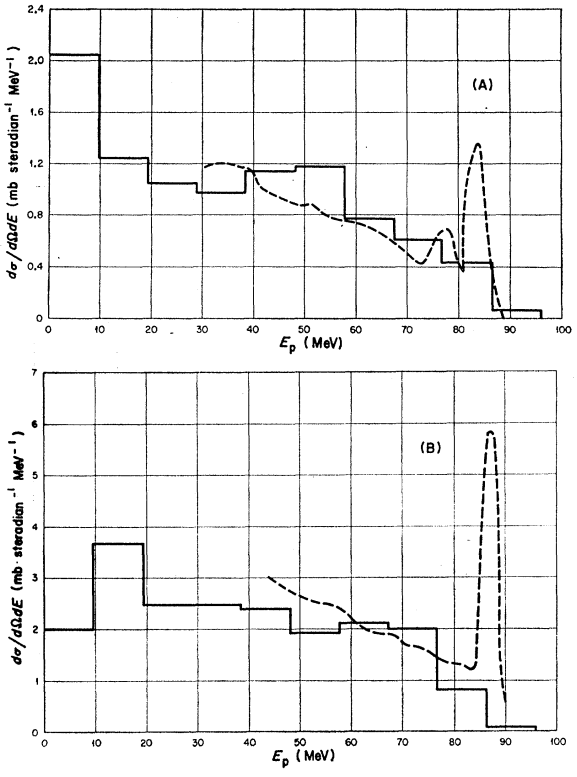

FIG. 7. Proton spectra at 40° from 96-MeV protons on (A) F and (B) Bi. Dashed curve: experimental results of K. Strauch and F. Titus [Phys. Rev. **104**, 191 (1956)]; solid lines: calculated spectrum of protons emitted in the angular interval 30° to 50°.

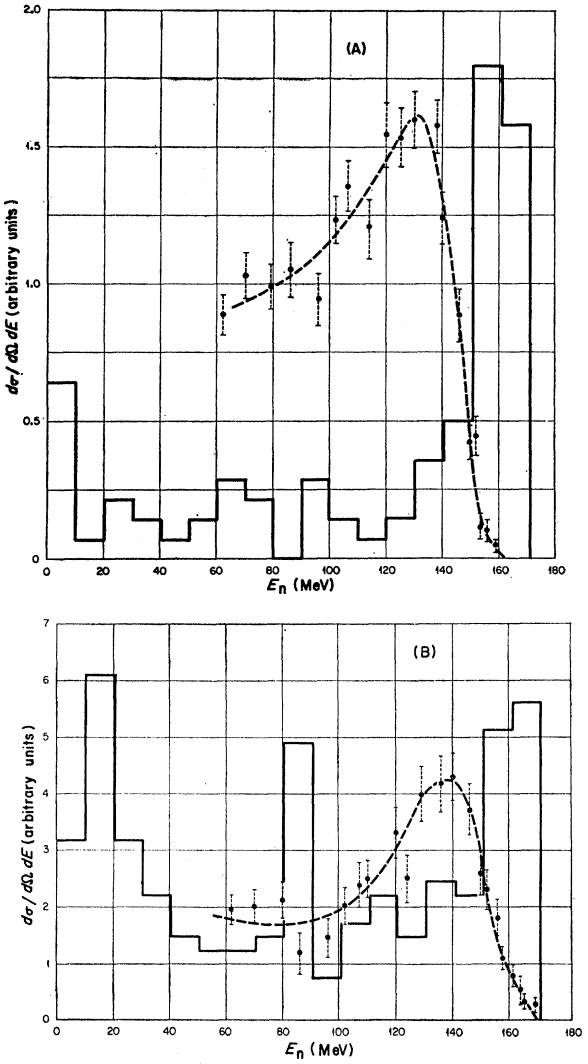

FIG. 8. Neutron spectra at 2.5° from 171-MeV protons on (A) C and (B) U. Dashed curve: Cassels' experimental results [J. M. Cassels *et al.*, Phil. Mag. **42**, 215 (1951)]; solid lines: calculated spectrum of neutrons emitted in the angular interval 0° to 15°. The units of the ordinate are arbitrary.

Frequency Distribution of Cascade Products

A comparison of the frequency distribution of cascade products for 170-MeV protons on Cu^{64} indicates that the results for both configurations in this calculation

[15] Space limitations have led to the decision to publish these comparisons as a document of the ADI Auxiliary Publication Project, Photoduplication Service, Library of Congress, Washington, D.C. A copy may be obtained by referring to the Document No. 7584, and by sending $2.50 for photoprints or $1.75 for 35-mm microfilm. Advance payment is required. Make checks or money orders payable to: Chief, Photoduplication Service, Library of Congress.

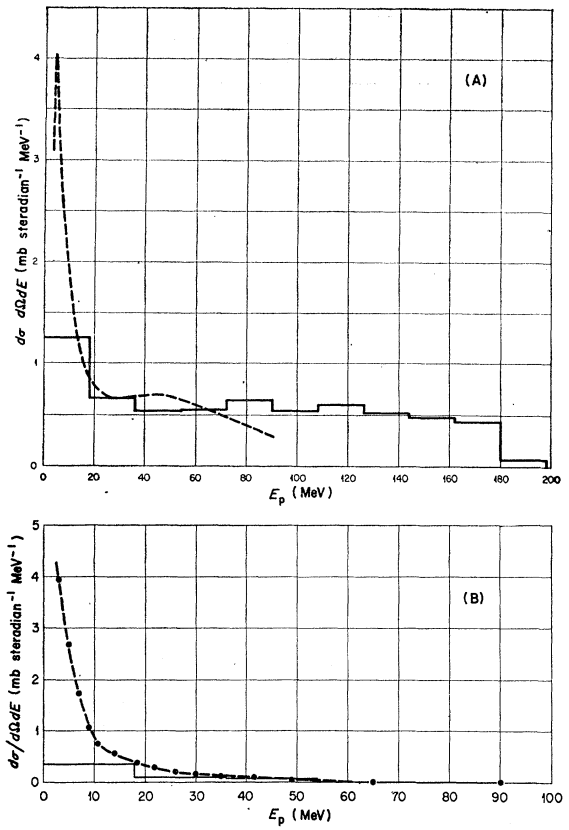

FIG. 9. Proton spectra from (A) 0° to 65° and (B) 100° to 180° for 190-MeV protons on Al. Dashed curve: Bailey's experimental results [L. E. Bailey, University of California Radiation Laboratory Report UCRL-3334, 1956 (unpublished)]; solid lines: calculated spectrum.

are very similar to the results of Metropolis *et al.* (Ref. 3, Fig. 4).

Fast Prong Distributions

The comparison of the fast prong distribution for 375-MeV protons on Ru^{100} indicates that the results are sensitive to the configuration. Use of the small, uniform configuration yields results that are almost identical to those given by Metropolis *et al.* (Ref. 3, Table III) and compare favorably with the experimental data, while use of the standard configuration enhances the escape of one fast proton (see Table III, this paper).

Angular Distributions

The angular distributions of protons with energies greater than 90 MeV from 286-MeV protons on Ru^{100} calculated by Metropolis *et al.* (Ref. 3, Fig. 6) are very similar to those obtained with both configurations in the present calculation.

Proton Spectra at Various Angles

Comparisons of the proton spectra at a few angles in the forward hemisphere for 83-MeV neutrons on Cu^{64} show that for angles less than 30° the spectra for the standard configuration have high-energy peaks, whereas those for the small, uniform configuration and those given by Metropolis *et al.* (Ref. 3, Fig. 8) exhibit no such peaks. This difference is discussed later. The spectrum values for the small, uniform distribution are roughly 25 to 50% smaller than those of Metropolis *et al.* at some energies, but the shapes are very nearly the same.

Transparency

Transparencies calculated for 82- and 286-MeV protons on $_{29}Cu^{64}$ and $_{82}Pb^{207}$ were used for comparison with those calculated by Metropolis *et al.* for protons on $_{29}Cu^{64}$ and $_{83}Bi^{209}$ (Ref. 3, Table V). Similarly, 82- and 286-MeV neutrons on $_{29}Cu^{64}$ were compared. Except for one case, the results for the small, uniform configuration are within the statistics published in Ref. 3. The transparencies for the standard configuration will clearly be different.

Average Number of Cascade Particles Emitted for Incident Protons

Comparisons of the average number of cascade particles emitted for 82- and 286-MeV protons incident

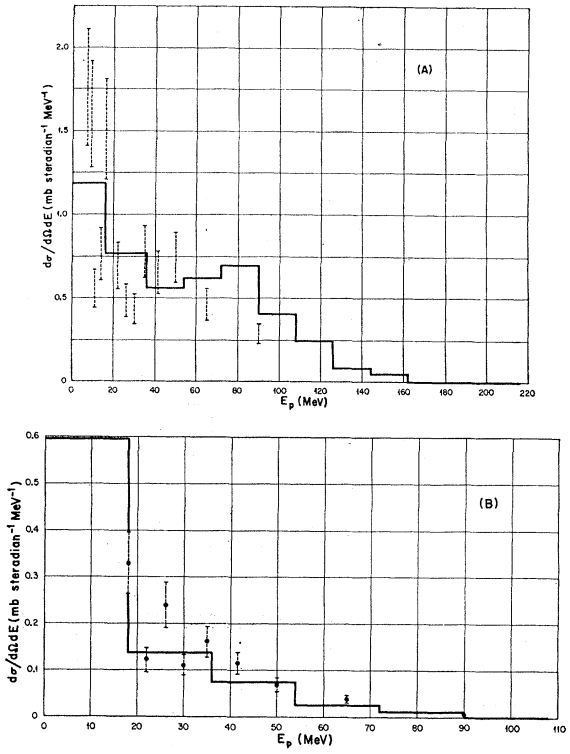

FIG. 10. Proton spectra from (A) 46° to 65° and (B) 102° to 117° for 190-MeV protons on Al. Error bars: Bailey's experimental results [L. E. Bailey, University of California Radiation Laboratory Report UCRL-3334, 1956 (unpublished)]; solid lines: calculated spectrum.

on various nuclei manifest the effect of the different cutoff energies used in the two calculations. In the technique used by Metropolis *et al.* (results given in Fig. 12 of Ref. 3), the cutoff energy measured with respect to the outside of the nucleus is greater for cascade protons than for neutrons. In the present calculation, the cutoff energy is the same for both particles; however, the cutoff energy measured with respect to the outside of the nucleus for the small, uniform configuration turned out to be a little smaller than the cutoff energy for neutrons used by Metropolis *et al.* Therefore, calculations of the average number of cascade neutrons emitted yielded values for both configurations that are slightly greater, in most cases, than those obtained by Metropolis *et al.*, whereas calculations of the average number of protons emitted yielded values for both configurations that are definitely higher (about 10 to 30%) than those obtained by Metropolis *et al.*

Excitation Energies

For incident nucleons, the excitation energy was calculated from the expression

$$E^*=T_i-T_0-7(n-1),$$

where T_i is the kinetic energy of the incident particle,

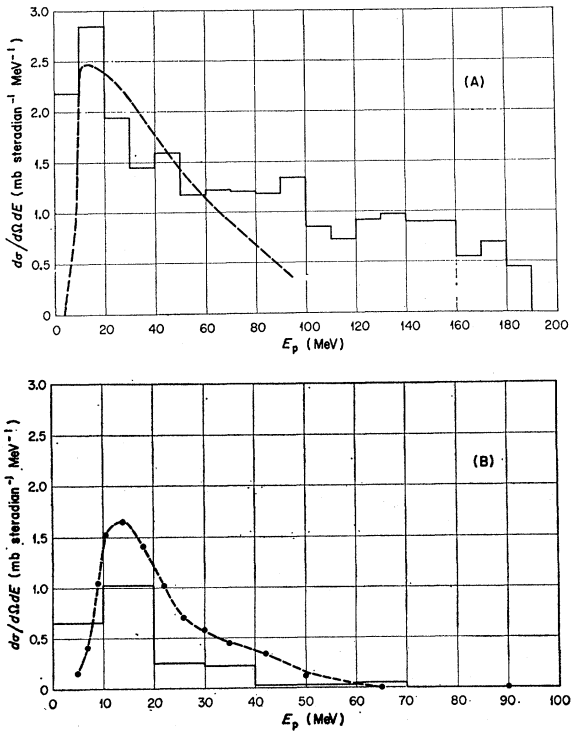

FIG. 11. Proton spectra from (A) 0° to 65° and (B) 100° to 180° for 190-MeV protons on Au. Dashed curve: Bailey's experimental results [L. E. Bailey, University of California Radiation Laboratory Report UCRL-3334, 1956 (unpublished)]; solid lines: calculated spectrum.

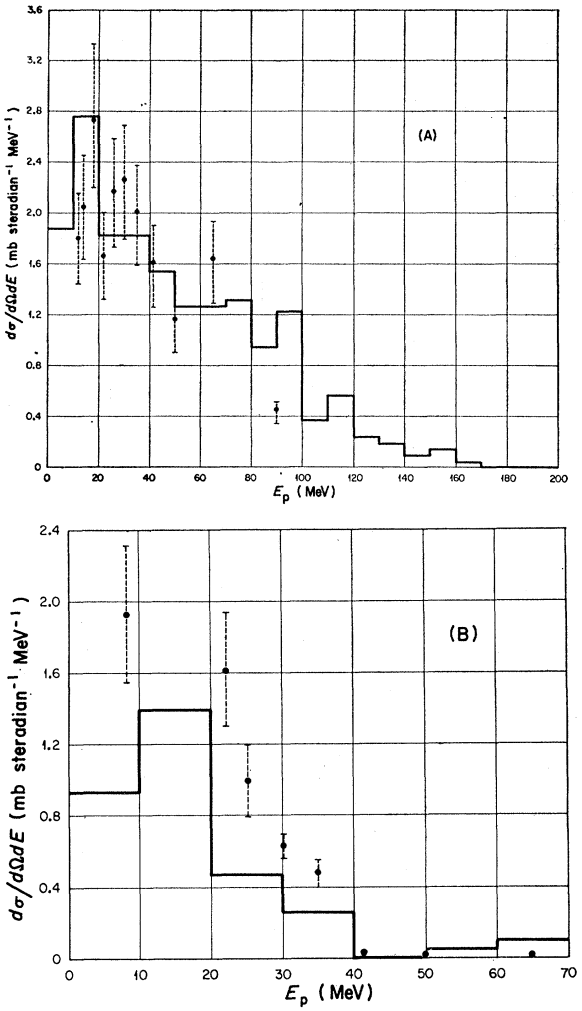

FIG. 12. Proton spectra from (A) 46° to 65° and (B) 102° to 117° for 190-MeV protons on Au. Circles: Bailey's experimental results [L. E. Bailey, University of California Radiation Laboratory Report UCRL-3334, 1956 (unpublished)]; solid lines: calculated spectrum.

T_0 is the sum of the kinetic energies of the emitted cascade particles, n is the number of emitted particles, and 7 (MeV) is the binding energy of the most loosely bound nucleon (assumed to be constant for all nuclei).

Comparisons of the excitation-energy distributions for 82- and 286-MeV protons on $_{29}Cu^{64}$ and $_{82}Pb^{207}$ with those of Metropolis *et al.* for $_{29}Cu^{64}$ and $_{83}Bi^{209}$ (Ref. 3, Fig. 15) show that while the general shapes of the distributions for the small, uniform configuration compare favorably with those of Metropolis *et al.*, the peaks in the distributions are shifted (20 to 40 MeV) to higher energies. This is probably due to the difference in the basic sampling techniques used in the two calculations. Any differences in the nucleon-nucleon cross sections that were used appear to be small, and if the cutoff energy is increased in the present calculation to correspond more closely to that used by Metropolis

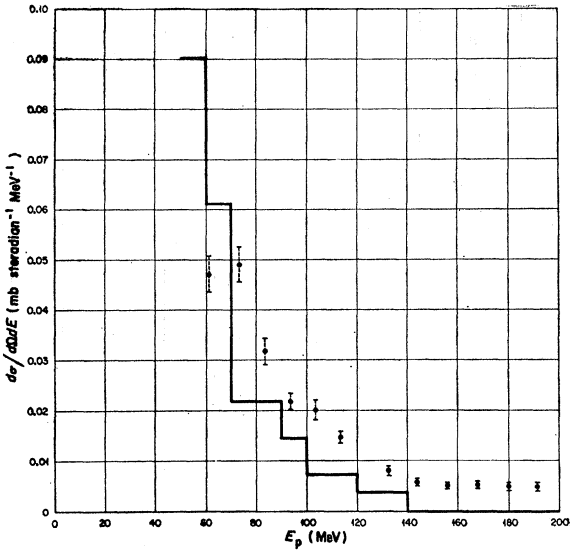

FIG. 13. Proton spectra at 90° from 240-MeV protons on C. Points: Temmer's experimental values [G. M. Temmer, Phys. Rev. **83**, 1067 (1951)]; solid lines: calculated spectrum for protons emitted in the angular interval 70° to 110°.

et al. the excitation-energy spectrum is shifted to higher energies. The excitation-energy distributions obtained with the standard configuration are somewhat different than those of Metropolis *et al.*, particularly at the low excitation energies, where the value of the distribution is greater. This is a result of the lower average density of the standard configuration, for there is an increased probability that incident particles will make single collisions and then escape, leaving less energy for excitation. The shape of the spectrum for the standard configuration is somewhat different than that of Metropolis *et al.*, but the average excitation energies are very similar.

The average excitation energies resulting from the escape of several specific combinations of cascade particles were calculated for protons on $_{29}Cu^{64}$ and $_{82}Pb^{207}$, as above. In almost every case the results from both configurations used in this calculation are within the statistical limits published by Metropolis *et al.* (Ref. 3, Tables IX and X).

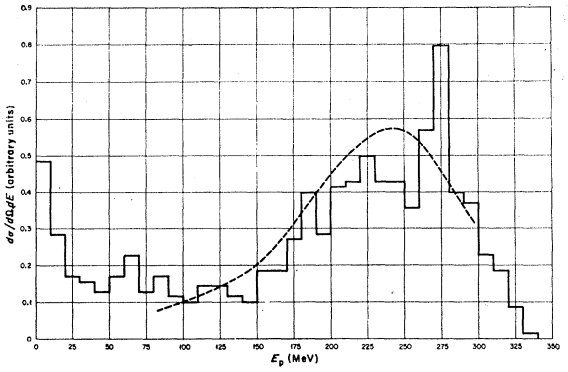

FIG. 14. Proton spectra at 30° from 340-MeV protons on C. Dashed curve: Cladis' experimental spectrum [J. B. Cladis, W. N. Hess, and B. J. Moyer, Phys. Rev. **87**, 425 (1952)]; solid lines: calculated spectrum of protons emitted in the angular interval 20° to 40°. The units of the ordinate are arbitrary.

Number of Cascade Pions and Nucleons for Incident π^- and π^+

For 50- and 134-MeV π^- and 210-MeV π^+ on Ru^{100}, calculations for both the small, uniform configuration and the standard configuration yield a considerably higher number of cascade pions (10 to 70%) than the calculations of Metropolis *et al.* The number of cascade nucleons, however, is smaller (30%) for 50-MeV π^- and slightly smaller (~8%) for 134-MeV π^-. The inclusion of the pion potential in the present calculation and the difference in the sampling techniques are

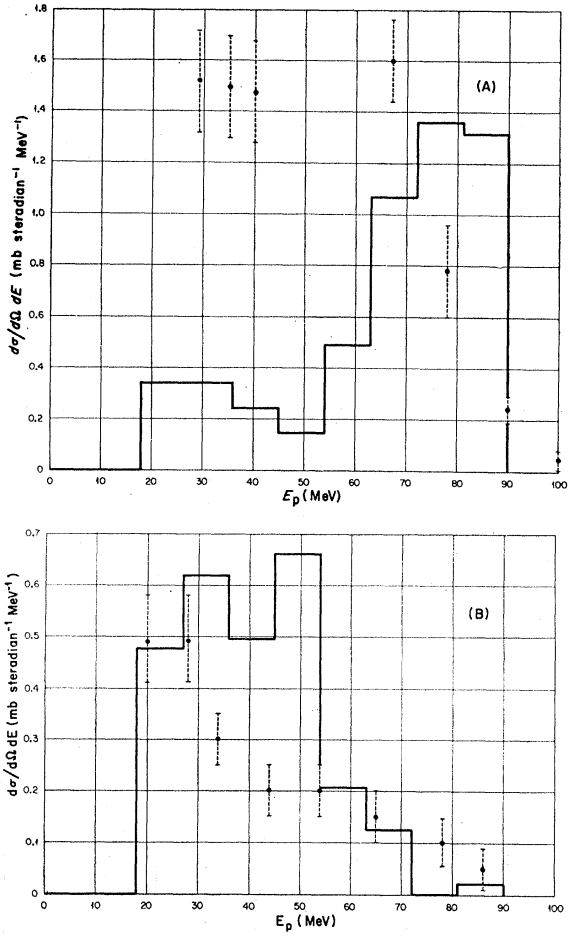

FIG. 15. Proton spectra at (A) 0° and (B) 45° for protons with energies greater than 20 MeV from 90-MeV neutrons on C. Points: experimental results of Hadley and York [J. Hadley and H. York, Phys. Rev. **80**, 345 (1950)]; solid lines: calculated spectrum of protons emitted in the angular intervals 0° to 25° and 36° to 54° for (A) and (B), respectively.

calculational differences—probably magnified by the pion-nucleon resonance—which very likely lead to the discrepancy in the pion multiplicities.

COMPARISON WITH EXPERIMENT: INCIDENT NUCLEONS

Nonelastic Cross Sections

The term "nonelastic cross section" used here refers to the cross section for all events which are not pure elastic scattering. Comparisons of typical data from the calculations with experimental nonelastic cross sections for incident neutrons and protons (Table I) show good agreement. The calculations of Metropolis *et al.*[3] for incident protons were also in good agreement with the experimental data with which they were compared.

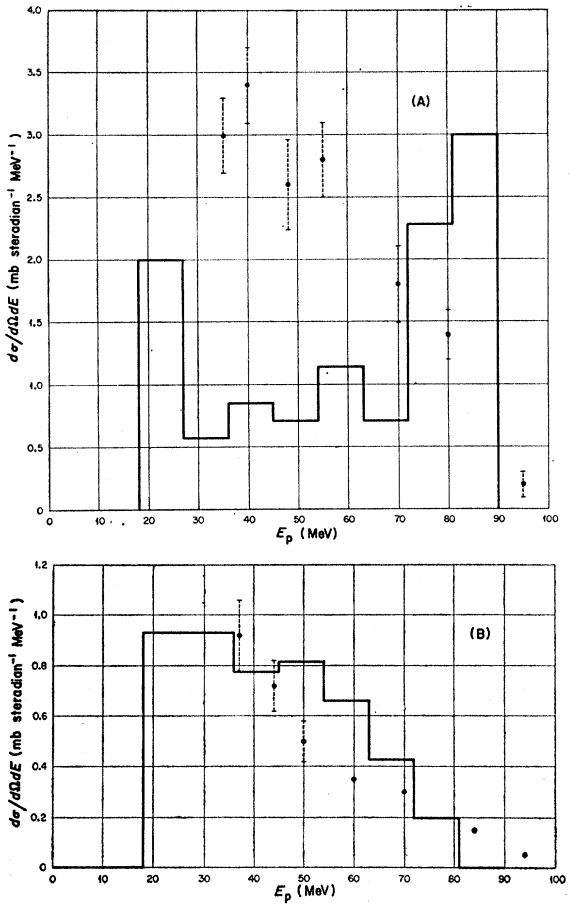

FIG. 16. Proton spectra at (A) 0° and (B) 45° for protons with energies greater than 20 MeV from 90-MeV neutrons on Cu. Points: experimental results of Hadley and York [J. Hadley and H. York, Phys. Rev. **80**, 345 (1950)]; solid lines: calculated spectrum of protons emitted in the angular intervals from 0° to 20° and 36° to 54° for (A) and (B), respectively.

Average Excitation Energy

The average excitation energy for 190-MeV protons on various nuclei has been deduced from experimental data by Gross.[16] As shown in Table II, his results are in good agreement with the calculated values. Similar comparisons made by Metropolis *et al.* for incident protons also showed good agreement.

TABLE I. Nonelastic cross sections for protons and neutrons incident on various nuclei.

Incident particle	Energy (MeV)	Target	Nonelastic cross section (mb) Calculated[a]	Experimental[b]
Proton	185	Be	187±7	172±17
	305		176±7	151±15
	185	Al	417±9	408±41
	305		394±11	334±33
	170	Cu	795±23	
	185			746±75
	240		747±23	667±67
	185	U	1825±38	1900±190
	305		1754±28	1600±160
Neutron	95	Be	217±7	210±8[c]
	84	Al	502±16	500±50[d]
	300		383±11	390±23
	84	Cu	825±23	910±50[d]
	300		725±16	755±33
	84	Pb	1654±26	1850±180[d]
	300		1552±27	1720±80

[a] Errors shown are the limits for the standard 68% confidence interval.
[b] Unless otherwise noted, all the data comes from G. P. Millburn, W. Birnbaum, W. E. Crandall, and L. Schecter, Phys. Rev. **95**, 1268 (1954).
[c] P. E. Hodgson, Nucl. Phys. **21**, 21 (1960).
[d] Upper limit.

Spectra of Cascade Particles

Comparisons of calculated and experimental spectra of cascade particles for incident protons are shown in Figs. 6–14, in the order of increasing proton energy, and for incident neutrons in Figs. 15 and 16. In most cases the agreement is good. In Fig. 7 the high-energy experimental peaks are due to elastic scattering or nuclear structure, and the comparisons should be made with the nonelastic continuum. In Figs. 9 and 10 the low-energy peaks result from nuclear evaporation, and the comparisons are valid for energies greater than about 15 MeV. Although Figs. 11 and 12 contain the same type of data as Figs. 9 and 10, there is very little evaporation associated with the data of Figs. 11 and 12 because the potential barrier of gold is so high.

TABLE II. Average excitation energies for 190-MeV protons incident on various nuclei.

Element	Average excitation energy (MeV) Calculated	Experimental[a]
C	22	27±5
Al	36	50±8
Ni	59	57±9
Ag	72	69±12
Au	92	83±17
U	95	88±18

[a] See Ref. 16.

[16] E. Gross, UCRL-3330, 1956 and UCRL-3337, 1956 (unpublished).

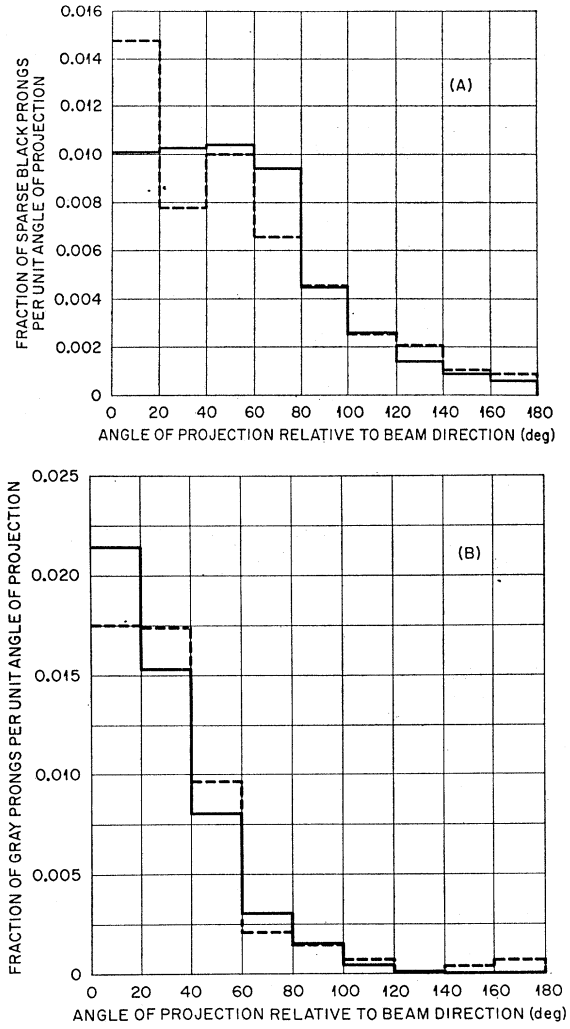

FIG. 17. Angular distribution of prongs from 300-MeV neutrons on heavy emulsion nuclei; (A) sparse black prongs (B) gray prongs. Dashed lines: experimental results of Bernardini [G. Bernardini, E. T. Booth, and S. J. Lindenbaum, Phys. Rev. **85**, 826 (1952)]; solid lines: calculated distributions from 300-MeV neutrons on Ru^{100} for protons emitted with energies 30 to 100 MeV and 100 to 300 MeV for (A) and (B), respectively.

One of the discrepancies between the calculated values and some of the experimental results is indicated in Figs. 6, 15, and 16. For incident particles with energies less than 100 MeV, the calculations predict a high-energy peak in the cascade particle spectra at 0° for medium- to light-weight elements, while the experimental data illustrated here does not exhibit this peak. Very recent high-resolution data from Harwell[17] does indicate a high-energy peak for the neutron spectra at 0° from 143-MeV protons on various elements. The peak is located at about 120 MeV for most elements, indicating a process which leaves the residual nucleus in an excited state. Hence, results using the standard configuration correctly exhibit a high-energy peak in the spectrum at small angles, but the position of the peak is at higher energies than in the measured spectrum because the effects of nuclear structure are not accounted for in the calculation. When the small, uniform configuration is used, the peaks are suppressed.

Angular Distribution of Cascade Particles

Experimental and calculated angular distributions of protons emitted with various energies for 300-MeV neutrons incident on emulsions are compared in Fig. 17 and show good agreement. Ru^{100} was used in the calculation to simulate the heavy emulsion nuclei.

Figures 18–20 show similar comparisons for fast protons from 90-MeV neutrons incident on various elements. For the most part, the agreement here is also quite good, but the experimental data are those for which the high-energy peaks in the spectrum of particles emitted in the forward direction were not resolved.

Cascade-Particle Multiplicities

In the photographic plate work of Bernardini *et al.*[18] it was noted that in the fast-particle multiplicities there was almost a complete similarity between proton-induced tracks and neutron-induced tracks. This is not indicated by the calculations for either the standard configuration or the small, uniform configuration where 375-MeV protons and 300-MeV neutrons on Ru^{100} were used to simulate the experiment. The comparisons are illustrated in Table III for protons with energies greater than 30 MeV. Bernardini *et al.* have attributed this

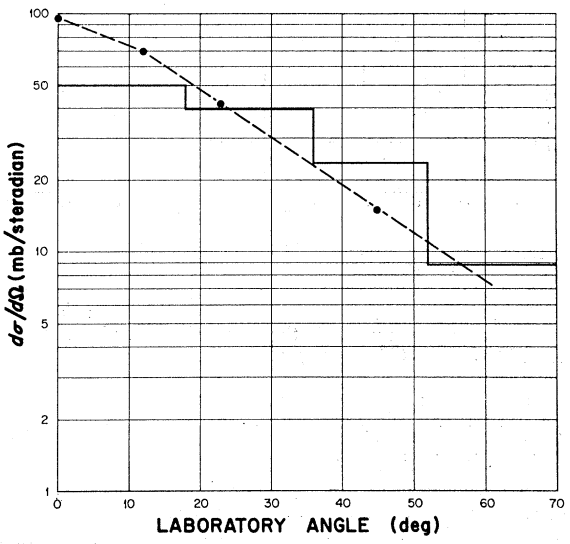

FIG. 18. Angular distribution of protons with energies greater than 20 MeV from 90-MeV neutrons on C. Dashed lines: experimental results of Hadley and York [J. Hadley and H. York, Phys. Rev. **80**, 345 (1950)]; solid lines: calculated distribution.

[17] P. H. Bowen, G. C. Cox, G. B. Huxtable, J. P. Scanlon, and J. J. Thresher, Nucl. Phys. **30**, 475 (1962).

[18] G. Bernardini, E. T. Booth, and S. J. Lindenbaum, Phys. Rev. **85**, 826 (1952).

TABLE III. Fast prong distributions for heavy emulsion nuclei.[a]

	Percentage of stars induced						
	By 375-MeV protons				By 300-MeV neutrons		
	Calculated				Calculated		
No. of fast prongs	Standard configuration	Small, uniform	Metropolis *et al.*	Experimental[b]	Standard configuration	Small, uniform	Experimental[b]
0	14	26	27.2±0.02	29±3	54	52	30±4
1	76	50	52.0±0.03	60±4	42	40	63±5
2	10	21	19.4±0.02	9±2	4	8	7±2
3	0.5	3	1.6±0.01	2±1	0	0.3	0

[a] Fast prongs indicate protons with energies greater than 30 MeV.
[b] See Ref. 18.

similarity of their experimental data to the average number of collision stages per event which they estimate to be two or three. The calculations indicate that this number is between one and two. Another experimental check on this point would be desirable.

(p,pn) Cross Sections

One of the more serious discrepancies between the calculated results of Metropolis *et al.*[3] and experimental data is that of the (p,pn) cross section. The calculated values were about a factor of 2 lower than those of the experiment for the $Cu^{65}(p,pn)Cu^{64}$ cross section, and calculations by Yule and Turkevich,[19] which were based on the work of Metropolis *et al.* gave cross sections that were a factor of 3 too small for the case of gold. The (p,pn) cross section is one of the values for which the effect of the diffuse edge was expected to be large.

In the present calculation a total of six nuclear configurations was used for each element to examine this effect. The configurations consisted of a uniform and a nonuniform density distribution for each of three outer nuclear radii identified as small, medium, and large. The small radius is given by $r=r_0A^{1/3}$, with $r_0=1.3$ F. The medium and large radii were determined from Hofstadter's Fermi-type distribution function[5] as the radii at which this function became 0.01 and 0.0001,

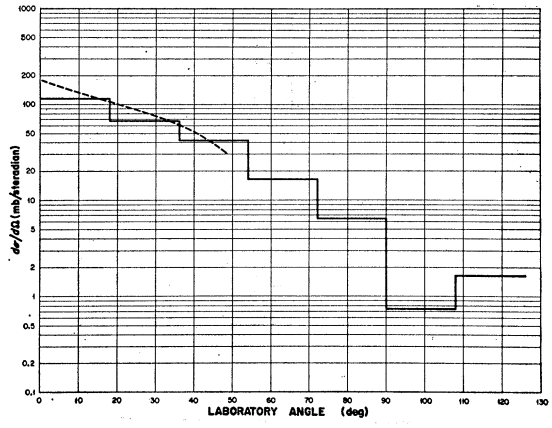

FIG. 19. Angular distribution of protons with energies greater than 20 MeV from 90-MeV neutrons on Cu. Dashed lines: Experimental results of Hadley and York [J. Hadley and H. York, Phys. Rev. **80**, 345 (1950)]; solid lines: calculated distribution.

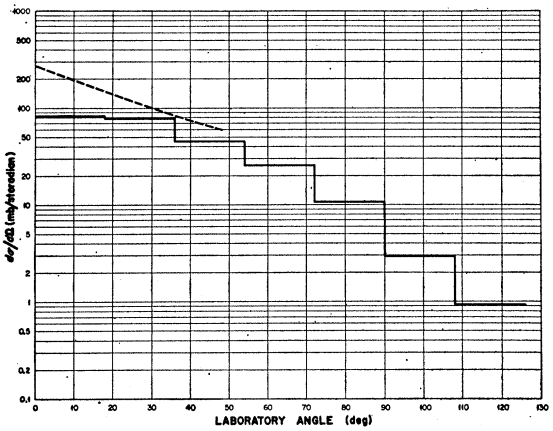

FIG. 20. Angular distribution of protons with energies greater than 20 MeV from 90-MeV neutrons on Pb. Dashed lines: Experimental results of Hadley and York [J. Hadley and H. York, Phys. Rev. **80**, 345 (1950)]; solid lines: calculated distribution.

respectively, of its central value. The large-radius configuration was used to examine the effects of an extreme edge. The medium-radius nonuniform density distribution is the standard configuration used elsewhere in this report. The small-radius uniform distribution corresponds to the configuration used in the work of Metropolis *et al.* These configurations are illustrated in Fig. 21.

The output from the cascade code was transformed into suitable input data from an evaporation code that was written by Dresner[20] and incorporates the work of Dostrovsky *et al.*[21] The input data included the atomic number, the mass number, and the excitation energy of the nucleus at the completion of the cascade.

The resulting cross sections are compared with experimental data of Yule and Turkevich[19] in Tables

[19] H. P. Yule and A. Turkevich, Phys. Rev. **118**, 1591 (1960).

[20] L. Dresner, ORNL-CF-61-12-30, 1961 (unpublished).

[21] S. Dostrovsky, Z. Fraenkel, and G. Friedlander, Phys. Rev. **116**, 683 (1959).

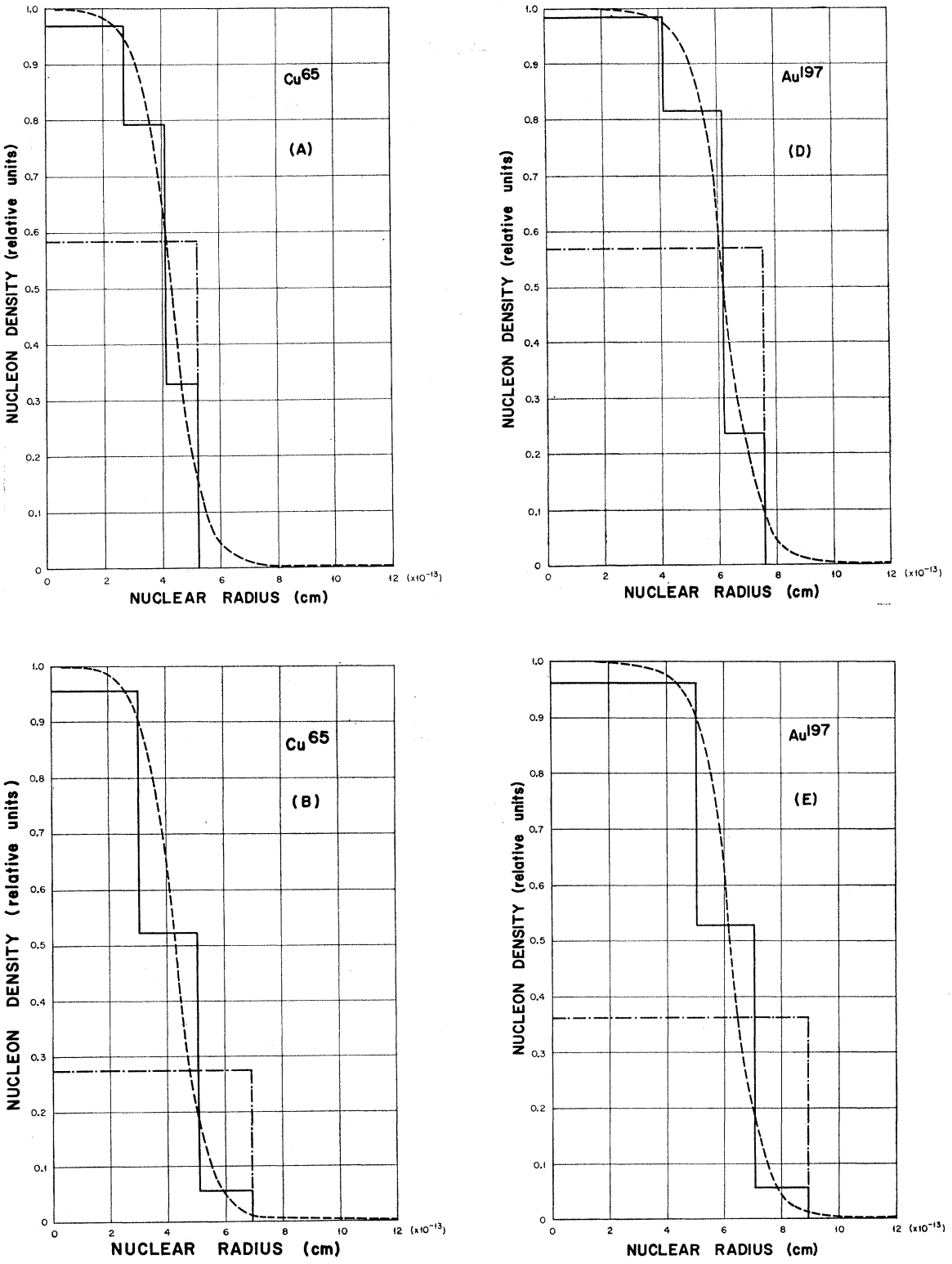

FIG. 21. Various nucleon density distribution within the nucleus for Cu and Au; (A) and (D) small nuclear radius, (B) and (E) medium nuclear radius. Solid lines: nonuniform configuration; dash-dotted lines: uniform configuration; dashed line: Hofstadter's curve (see Ref. 5).

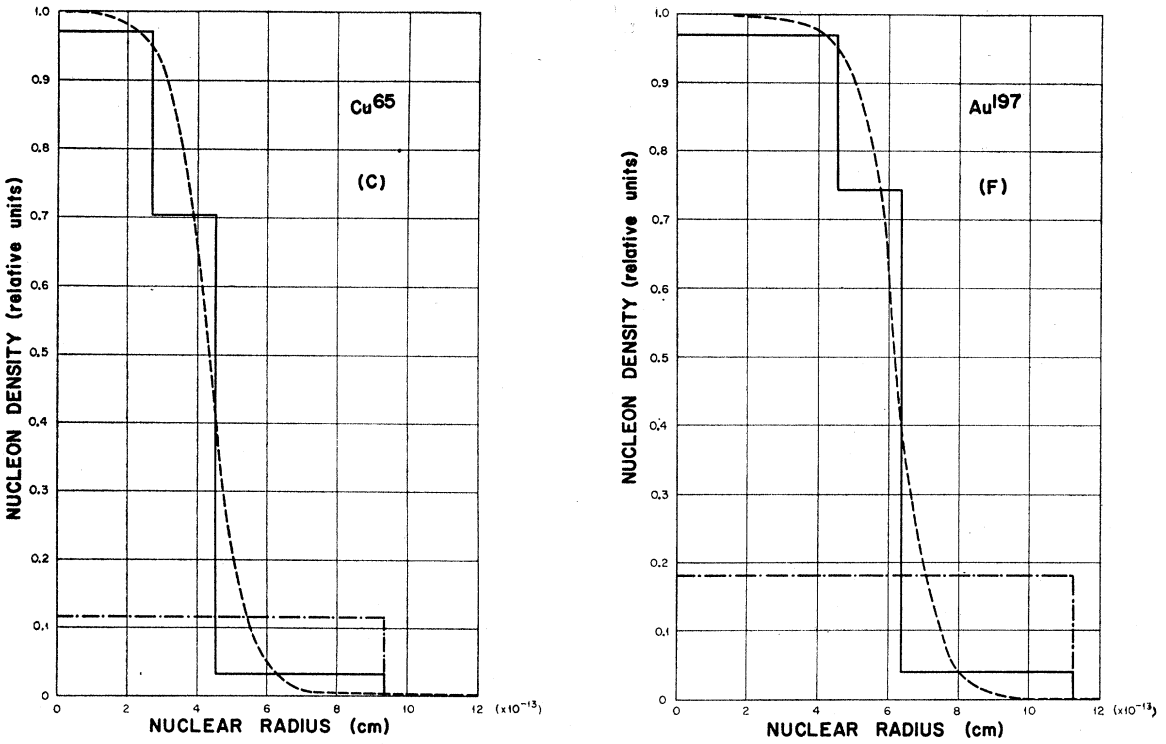

FIG. 21 (*continued*). Various nucleon density distributions within the nucleus for Cu and Au; (C) and (F) large nuclear radius. Solid lines: nonuniform configuration; dash-dotted lines: uniform configuration; dashed line: Hofstadter's curve (see Ref. 5).

IV and V, from which the following conclusions can be drawn:

(1) The effect of nuclear size on this reaction is generally greater than the effect of nuclear edge.

(2) With the nuclear volume kept constant, the expected increase in the cross section as the density is changed from a uniform to a nonuniform distribution occurs consistently only in the case of gold.

(3) The change in the cross section in going to the diffuse edge was only partially successful in accounting for the discrepancy with experiment.

A total of 9000 incident particle histories were used for each standard configuration and 4000 histories were used for each of the others.

This cross section appears to be very sensitive to the nuclear model, and it is the author's opinion that it is

TABLE IV. Cross sections for the $Cu^{65}(p,pn)Cu^{64}$ reaction and for the total nonelastic scattering as a function of proton energy and nuclear configuration.

Proton energy (MeV)	Nuclear configuration	(p,pn) Cross section (mb) Calculated	(p,pn) Cross section (mb) Experimental[a]	Calculated nonelastic cross section (mb)	(p,pn) Cross section/nonelastic cross section for calculated quantities
82	Small, uniform	26±2	108.4±4.2	740	0.0351
	Small, nonuniform	32±3		701	0.0457
	Medium, uniform	72±3		1119.0	0.0643
	Medium, nonuniform[b]	71±3		876	0.0811
	Large, uniform	224±12		1751	0.1279
	Large, nonuniform	183±11		1087	0.1684
196	Medium, nonuniform[b]	54±4	64.3±2.5	763	0.0708
330	Small, uniform	21±2	55.9±2.2	693	0.0303
	Small, nonuniform	19±2		642	0.0296
	Medium, uniform	66±3		939	0.0703
	Medium, nonuniform[b]	51±3		750	0.0680
	Large, uniform	225±12		1272	0.1769
	Large, nonuniform	134±9		844	0.1588

[a] See Ref. 19.
[b] Standard nuclear configuration adopted for this report.

TABLE V. Cross sections for the $Au^{197}(p,pn)Au^{196}$ reaction and for the total nonelastic scattering as a function of proton energy and nuclear configuration.

Proton energy (MeV)	Nuclear configuration	(p,pn) Cross section (mb) Calculated	Experimental[a]	Calculated nonelastic cross section (mb)	(p,pn) Cross section/nonelastic cross section for calculated quantities
82	Small, uniform	13±2	121.6±9.8	1669	0.0078
	Small, nonuniform	23±3		1534	0.0150
	Medium, uniform	15±2		2139	0.0070
	Medium, nonuniform[b]	58±4		1737	0.0334
	Large, uniform	98±10		3411	0.0287
	Large, nonuniform	182±13		2229	0.0817
210	Medium, nonuniform[b]	49±4	73.6±6.0	1553	0.0316
282	Small, uniform	10±2	71.0±5.7	1582	0.0063
	Small, nonuniform	18±3		1427	0.0126
	Medium, uniform	31±3		1972	0.0157
	Medium, nonuniform[b]	50±4		1553	0.0322
	Large, uniform	131±11		2815	0.0465
	Large, nonuniform	166±13		1746	0.0951

[a] See Ref. 19.
[b] Standard nuclear configuration adopted for this report.

beyond the capacity of the present model to predict its value with an accuracy better than a factor of 2.

COMPARISON WITH EXPERIMENT: INCIDENT PIONS

Nonelastic Cross Sections

A comparison between calculated and experimental nonelastic cross sections for pions incident on various nuclei is given in Table VI. The calculated values are somewhat larger than the experimental values for the lightest elements. The calculations were repeated with absorption cross sections which were reduced by 50% at all energies, but this reduced the nonelastic cross section only ≈10%. In general, the agreement here is fair, but it is not as good or as consistent as the same comparisons for incident nucleons.

Energy Spectrum for Nonelastic Scattering

The energy spectrum for nonelastic scattering into various angular intervals for a few reactions are illustrated in Figs. 22 and 23. The data are rather coarse, but the agreement is reasonable.

One of the discrepancies between the results of Metropolis *et al.* and experimental data[22] is the nonelastic spectra at several angles for π^- on carbon and lead. The experiments indicated that the peaks in the spectra occur at much lower energies than were predicted by the calculation. Among suggested possible sources for the discrepancy were deficiencies of the nuclear model mentioned previously. This discrepancy was investigated in the present work at a few angles for π^- on lead using the present model with the six nuclear configurations described before. The comparisons are

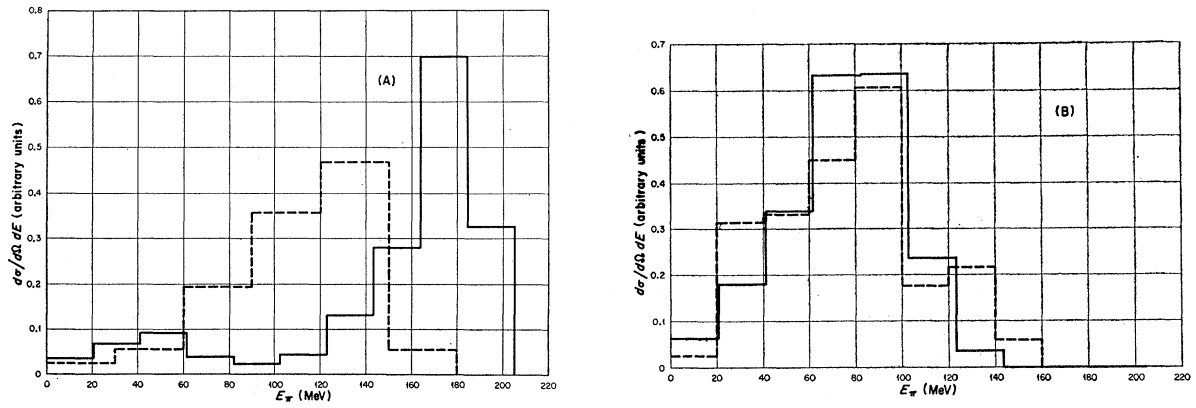

FIG. 22. Energy spectra of nonelastic π^+ emitted in the angular intervals (A) 0° to 60° and (B) 120° to 180° from 195 MeV π^+ on Li and C. Dashed lines: Petrov's experimental results (see Ref. 13); solid lines: calculated spectrum. Units of the ordinate are arbitrary.

[22] R. H. Miller, Nuovo Cimento **6**, 882 (1957).

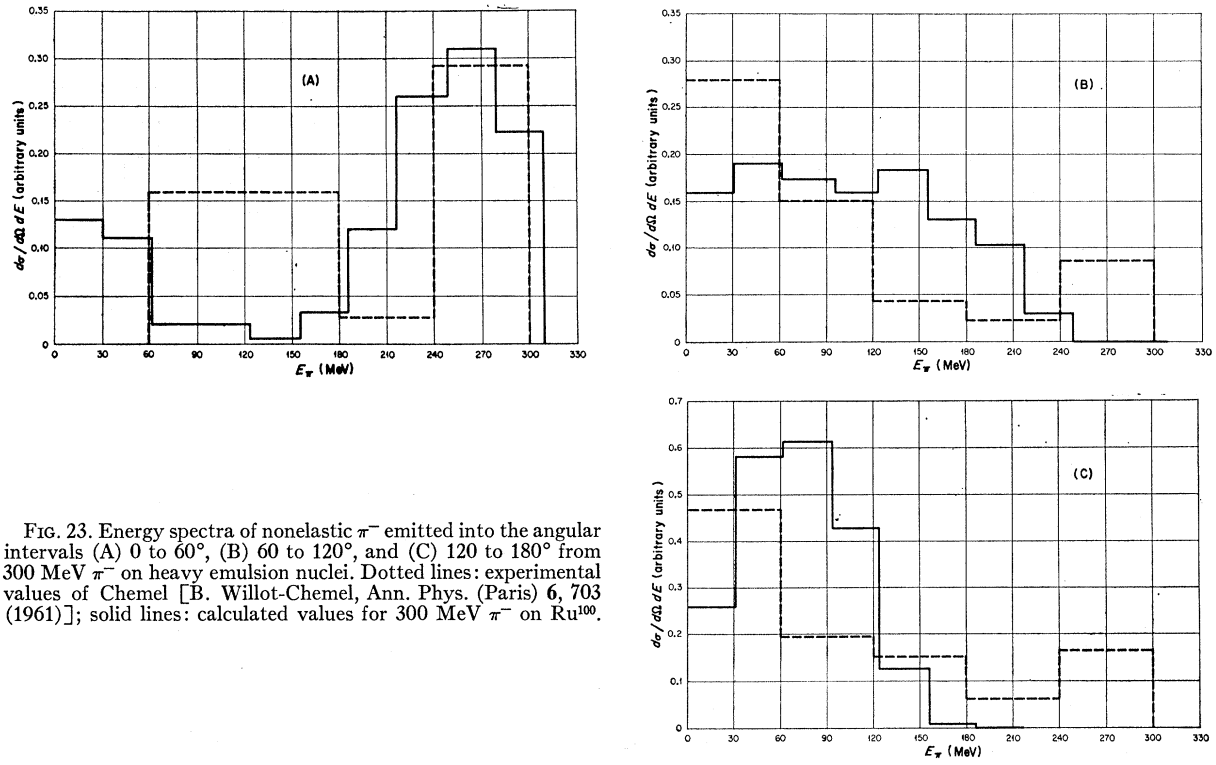

FIG. 23. Energy spectra of nonelastic π^- emitted into the angular intervals (A) 0 to 60°, (B) 60 to 120°, and (C) 120 to 180° from 300 MeV π^- on heavy emulsion nuclei. Dotted lines: experimental values of Chemel [B. Willot-Chemel, Ann. Phys. (Paris) **6**, 703 (1961)]; solid lines: calculated values for 300 MeV π^- on Ru^{100}.

given in Figs. 24 and 25. The discrepancy persists. The calculation was repeated for the standard configuration with the absorption cross section reduced by 50% at all energies, and the sole effect was to increase the sharpness of the peaks without shifting them. The data from the experiments imply a large energy transfer between the pion and the nucleus, which is not accounted for in the calculation.

Another discrepancy, although not a very large one, between the previous calculations and the experimental data[23] is the spectrum of pions nonelastically scattered into the backward hemisphere by the heavy nuclei in emulsions. It was suggested by Metropolis *et al.*[4] that the inclusion of a pion potential might account for this discrepancy. Although the present calculation did include a pion potential, the extent of its effect cannot be determined. The agreement with the experimental data is best for the nuclear configuration with the small radius, but it is also quite reasonable for the standard configuration, as is illustrated in Fig. 26.

TABLE VI. Total nonelastic cross sections for pions incident on various nuclei.

Pion	Energy (MeV)	Target	Nonelastic cross section (mb) Calculated[a]	Experimental
π^+	195	Li	324±10	226±18[b]
	195	C	455±11	325±26[b]
	270		358±10	296^{+35}_{-28}[c]
	50	Pb	1563±26	1620[d]
π^-	125	C	458±11	308±43[e]
	150		478±11	430±42[f]
	225		423±11	346±21[g]
	225	Al	653±14	596±30[g]
	225	Cu	1038±19	1058±45[g]
	225	Sn	1471±20	1550±70[g]
	125	Pb	2062±29	2477±385[e]
	150		2145±29	2490±160[f]
	225		1993±29	2290±90[g]

[a] Errors indicated apply for a confidence coefficient of 68%.
[b] N. I. Petrov, V. G. Ivanov, and V. A. Rusakov (see Ref. 13).
[c] W. Kan Chang, Wang Tso-Tsiang, Ding Da-Tsao, L. N. Dubrovskii, E. N. Kladnitskaia, and M. I. Solov'ev, Zh. Eksperim. i Teor. Fiz. **35**, 899 (1958) [translation: Soviet Phys.—JETP **8**, 625 (1959)].
[d] Calculated from the mean free path in nuclear matter given by G. Saphir (see Ref. 27).
[e] See Ref. 28.
[f] See Ref. 22.
[g] V. G. Ivanov, V. T. Osipenkov, N. I. Petrov, and V. A. Rusakov, Zh. Eksperim. i Teor. Fiz. **31**, 1097 (1956) [translation: Soviet Phys.—JETP **4**, 922 (1957)].

Angular Distribution for Nonelastic Pion Scattering

Calculated and experimental angular distributions of nonelastically scattered pions are illustrated for a few cases in Figs. 27 and 28. The poorest agreement is that for π^- on lead as shown in Fig. 27. For this case the pions have lost more than 40 MeV, and it again illustrates the fact that there is a means of large energy transfer to the nucleus which is not represented by simple particle-particle collisions. In fact, the experimental data indicate a significant degree of isotropy for these events.

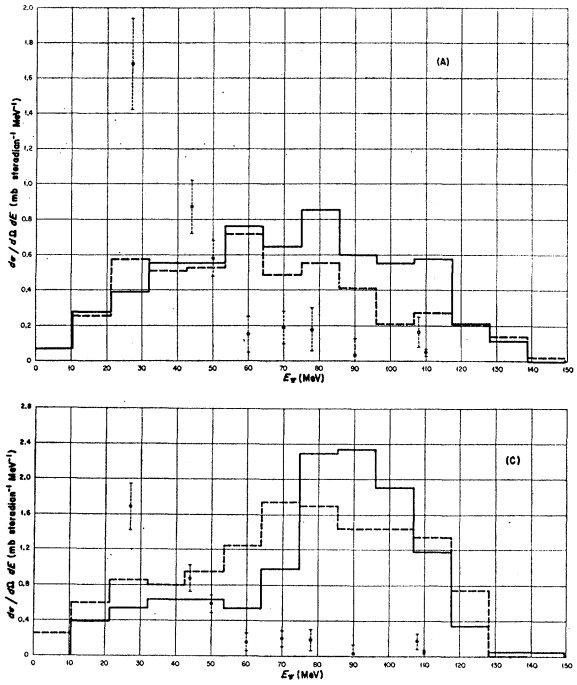

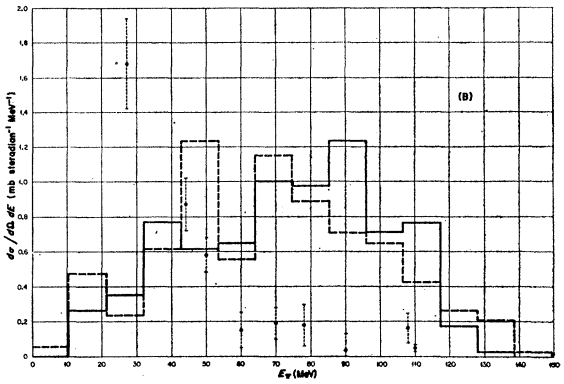

FIG. 24. Nonelastic π^- spectra at 90° from 150 MeV π^- on Pb. Calculated spectra for π^- in the interval 78° to 102° for nuclei with radius: (A) small, (B) medium, and (C) large. Solid lines: nonuniform nucleon-density distribution within the nucleus: dotted lines: uniform density distribution; circles: Miller'; experimental values (see Ref. 22).

The experimental angular distribution of nonelastically scattered pions of all energies from 162-MeV π^- on heavy emulsion nuclei[23] was in disagreement with the results of Metropolis *et al.* In the present calculation the disagreement was investigated with all six nuclear configurations, the results of which are illustrated in Fig. 29. In this case it is the configuration with the large radius that gives the best comparisons, but the agreement with the standard configuration is quite reasonable.

Pion Absorption

The experimental results of Azimov *et al.*[24] for the number of fast protons emitted in slow pion absorption

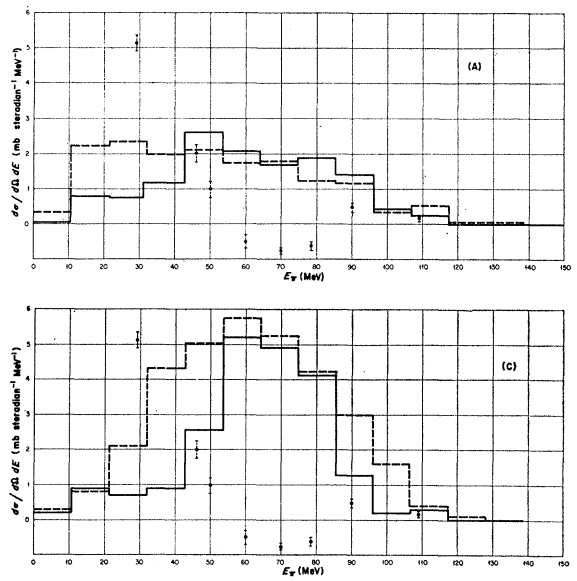

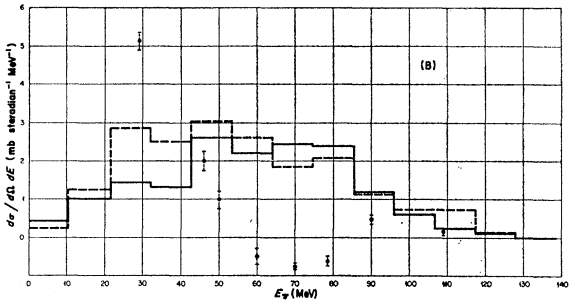

FIG. 25. Nonelastic π^- spectra at 138° from 150 MeV π^- on Pb. Calculated spectra for π^- in the interval 130° to 148° for nuclei with radius: (A) small, (B) medium, and (C) large. Solid lines: nonuniform nucleon density distribution within the nucleus; dotted lines: uniform density distribution; circles: Miller's experimental values (see Ref. 22).

[23] B. A. Nikol'skii, L. P. Kudrin, and S. A. Ali-Zade, Zh. Eksperim. i Teor. Fiz. **32**, 48 (1957) [translation: Soviet Phys.—JETP **5**, 93 (1957)].

[24] S. A. Azimov, U. G. Guliamov, E. A. Zamchalova, M. Nizametdinova, M. I. Podgoretskii, and A. Iuladeshev, Zh. Eksperim. i Teor. Fiz. **31**. 756 (1956) [translation: Soviet Phys.—JETP **4**, 632 (1957)].

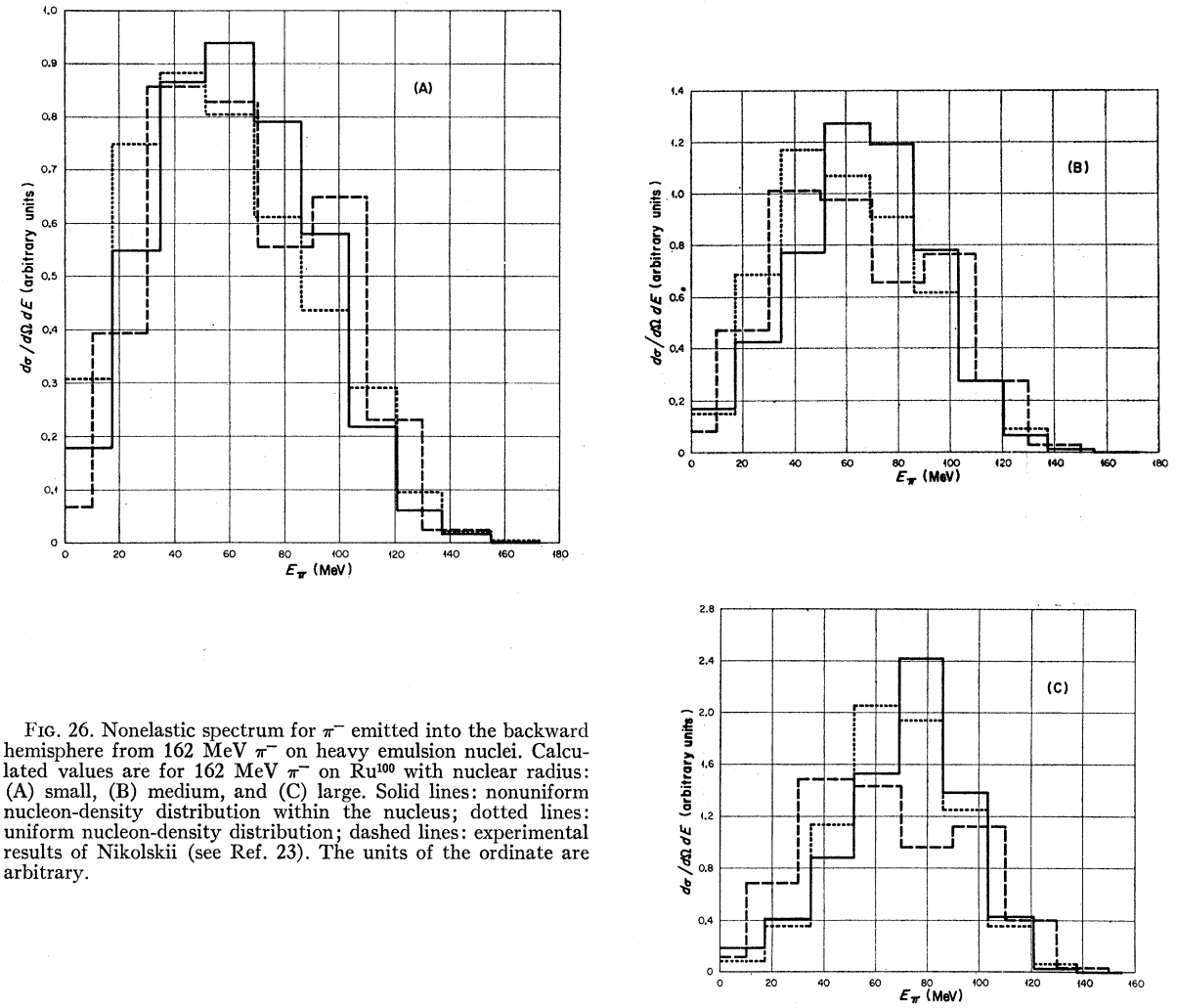

FIG. 26. Nonelastic spectrum for π^- emitted into the backward hemisphere from 162 MeV π^- on heavy emulsion nuclei. Calculated values are for 162 MeV π^- on Ru^{100} with nuclear radius: (A) small, (B) medium, and (C) large. Solid lines: nonuniform nucleon-density distribution within the nucleus; dotted lines: uniform nucleon-density distribution; dashed lines: experimental results of Nikolskii (see Ref. 23). The units of the ordinate are arbitrary.

in heavy-emulsion nuclei are compared with calculated results in Fig. 30. In the calculation slow π^- absorption was simulated by using 1-MeV π^- incident on Ru^{100}. This gives a rather uniform distribution of absorption events throughout the nucleus because the transparency is so high at this energy. The discrepancy in the shapes of the calculated and experimental spectra observed by Metropolis *et al.*[4] still persists even with a diffuse nuclear edge assumed in the present calculations.

The average number of protons per absorption emitted with energies greater than 30 MeV was calculated to be 0.09 with the diffuse edge; Metropolis *et al.* calculated a value of 0.18. The experimental value, obtained by applying the values estimated by Menon *et al.*[25] for the fraction of absorptions in heavy nuclei leading to "starless" tracks (31 starless tracks for every 54 producing stars) to the data of Azimov *et al.*, is 0.13. The value obtained by Metropolis *et al.* is higher than that of the present calculation because they assumed that absorption took place on *n-p* pairs and *p-p* pairs with equal probability, while in this calculation the probabilities were 0.73 and 0.27, respectively.

The calculation was repeated assuming that *n-p* pairs only were involved in the pion absorption. The fast proton spectrum obtained in this way was in excellent agreement with experiment, but the number of protons emitted per absorption with energy greater than 30 MeV was only 0.05.

A comparison of the calculated and experimental angular distributions of two protons resulting from the absorption of 50-MeV π^+ on carbon is shown in Fig. 31. This figure tends to support the claim of most experimentalists in this field that there are other mechanisms by which the pion is absorbed in addition to the two-particle cluster.

The calculated and experimental[26] π^+ absorption cross

[25] M. G. K. Menon, H. Muirhead, and O. Rachat, Phil. Mag. 41, 583 (1950).

[26] F. H. Tenney and J. Tinlot, Phys. Rev. 92, 974 (1953).

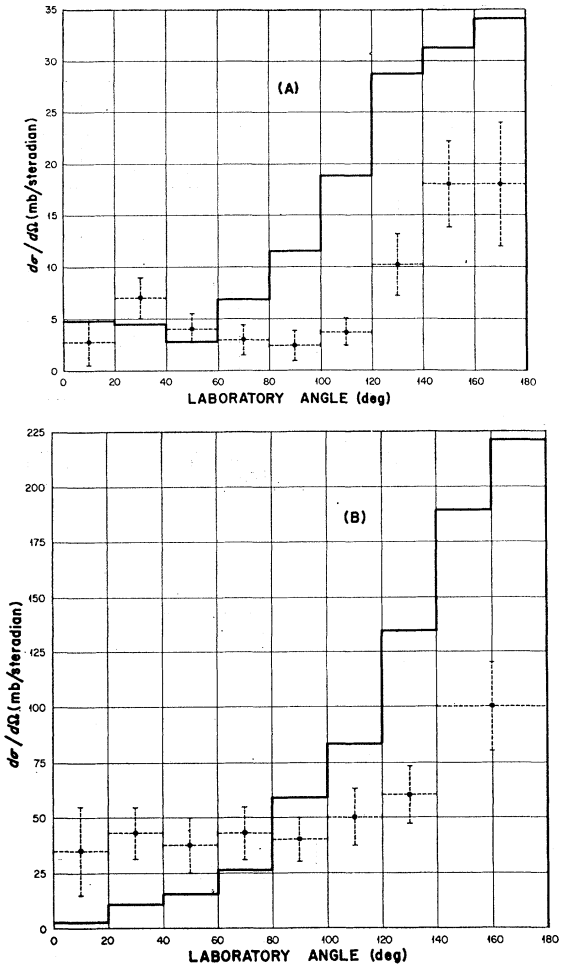

FIG. 27. Angular distribution of nonelastic π^- scattered with energy loss greater than 40 MeV for 125-MeV π^- on (A) C and (B) Pb. Points: experimental values of Kessler and Lederman (see Ref. 28); solid lines: calculated distribution.

sections for beryllium are shown in Table VII and indicate a fair agreement.

Pion Reactions Involving Charge Exchange

The largest discrepancies between the experimental results and the present calculations involve the charge-exchange cross section. A comparison of the charge-exchange cross sections alone is given in Table VIII. The statistics for this reaction in the experiment of

TABLE VII. Pion absorption cross sections for beryllium.

π^+ Energy (MeV)	Pion absorption cross section (mb) Calculated	Experimental[a]
20	58	56±9
30	63	74±13
40	67	96±20

[a] See Ref. 26.

TABLE VIII. Pion-charge-exchange cross sections.

Pion	Energy (MeV)	Target	Pion charge exchange cross section (mb) Calculated	Experimental
π^+	50	Pb	206	27±19[a]
π^-	125	C	61	$20\pm^{20}_{10}$[b]
π^-	125	Pb	215	$100\pm^{80}_{40}$[b]

[a] See Ref. 27.
[b] See Ref. 28.

Saphir[27] are rather poor, for he observed only two charge-exchange events out of 277 acceptable events.

The charge exchange cross sections can be further examined by comparing the results of calculations and experiments in which the sum of the charge exchange and absorption cross sections was obtained. The comparison is given in Table IX. Except for the last two entries, the agreement is quite good. The experimental cross section for 125-MeV π^- incident on lead[28]

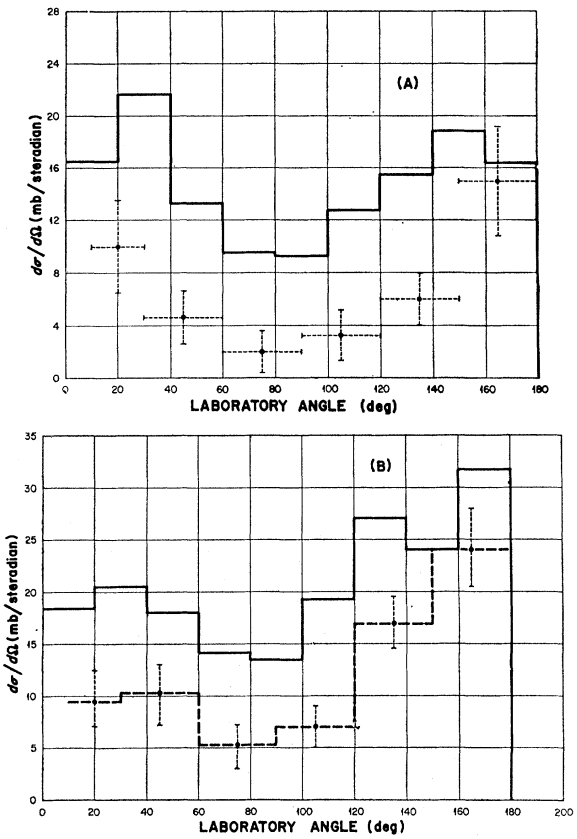

FIG. 28. Angular distribution of nonelastic π^+ from 195-MeV π^+ on (A) Li and (B) C. Points: experimental values of Petrov (see Ref. 13); solid lines: calculated spectrum. Calculated spectrum of graph (A) has been reduced by the ratio of the experimental to the calculated total nonelastic cross section.

[27] G. Saphir, Phys. Rev. **104**, 535 (1956).
[28] J. O. Kessler and L. M. Lederman, Phys. Rev. **94**, 689 (1954).

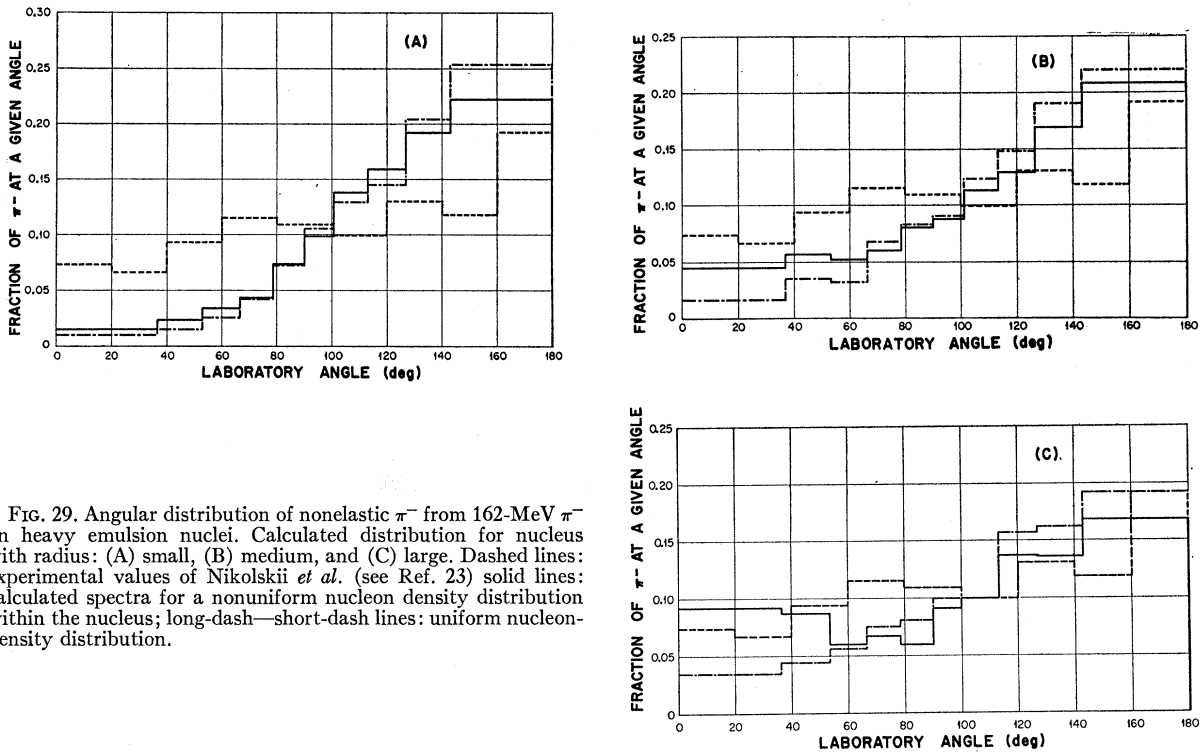

FIG. 29. Angular distribution of nonelastic π^- from 162-MeV π^- on heavy emulsion nuclei. Calculated distribution for nucleus with radius: (A) small, (B) medium, and (C) large. Dashed lines: experimental values of Nikolskii *et al.* (see Ref. 23) solid lines: calculated spectra for a nonuniform nucleon density distribution within the nucleus; long-dash—short-dash lines: uniform nucleon-density distribution.

was published as a "stars and stops" cross section which might include a considerable number of nonelastic collisions where the scattered particle is emitted with low energy.

Another comparison can be made of the ratio of the charge-exchange and absorption cross sections. Ratios calculated from the experimental data of Blinov *et al.*[29]

TABLE IX. Charge-exchange plus-absorption cross sections for various reactions.

Pion	Energy (MeV)	Target	Charge-exchange plus-absorption cross section (mb) Calculated	Experimental
π^+	195	Li	142	164±16[a]
π^+	78	C	174	195±20[b]
	195		205	203±22[a]
	270		146	165_{-22}^{+34}[c]
π^+	50	Pb	930	880±73[d]
π^-	125	C	206	220±40[e]
	150	C	209	192±34[f]
	125	Pb	923	1840±350[e]
	150	Pb	957	380±310[f]

[a] N. I. Petrov, V. G. Ivanov, and V. A. Rusakov (see Ref. 13).
[b] R. G. Salukvadze and D. Neagu, Zh. Eksperim. i Teor. Fiz. **41**, 78 (1961) [translation: Soviet Phys.—JETP **14**, 59 (1962)].
[c] W. Kan-Chang, Wang Tso-Tsiang, Ding Da-Tsao, L. N. Dubrovskii, E. N. Kladnitskii, and M. I. Solov'ev, Zh. Eksperim. i Teor. Fiz. **35**, 899 (1958) [translation: Soviet Phys.—JETP **8**, 625 (1959)].
[d] See Ref. 27.
[e] See Ref. 28.
[f] See Ref. 22.

[29] G. A. Blinov, M. F. Lomanov, Ia. Ia. Shalamov, V. A. Shebanov, and V. A. Shchegolev, Zh. Eksperim. i Teor. Fiz. **35**, 880 (1958) [translation: Soviet Phys.—JETP **8**, 609 (1959)].

for π^+ on freons (CCl_2F_2 and $CClF_3$) are shown with the present calculations for π^+ on F^{19} in Table X. Here again, a higher charge-exchange cross section is predicted by the calculation.

A final experiment that again illustrates this discrepancy is that of Krivitskii and Reut[30] who measured the π^+ production at 90° from 308-MeV π^- on carbon. They assumed that all the π^+ came from pion production. They measured a differential cross section of 0.21±0.11 mb/sr at 90° and, assuming that the cross section was isotropic, obtained a total cross section of 2.6±1.3 mb. Predictions from the calculation, in which pion production is not included and where the π^+ result from two-charge-exchange scatterings within the nucleus, are that the differential cross section at 90° is 0.84 mb/sr and that the total cross section is 8 mb. Both values are higher than the measurement.

The discrepancies between the calculations and experiments for charge exchange reactions are difficult to reconcile, for on a particle-particle basis this cross section is quite large.

ERRORS

The only error limits that have been indicated for the calculated values are those associated with the total nonelastic cross section and (p,pn) cross section.

[30] V. V. Krivitskii and A. A. Reut, Doklady Akad. Nauk. SSSR **112**, 232 (1957) [translation: Soviet Phys.—Doklady **2**, 24 (1957)].

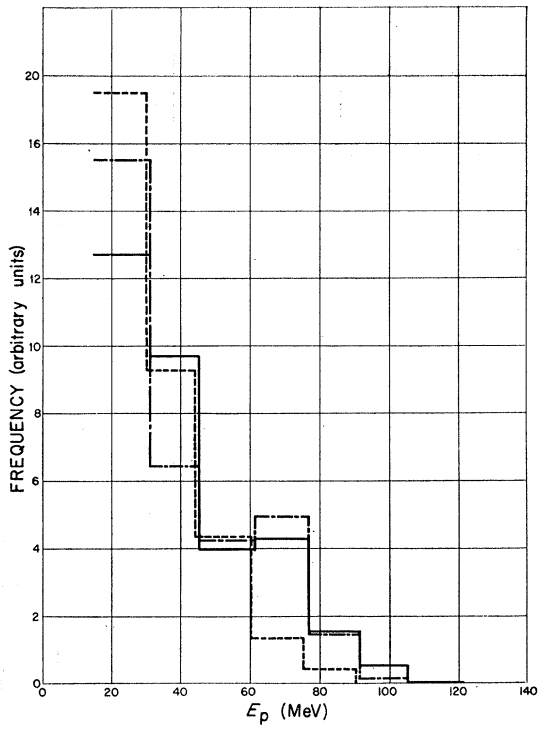

FIG. 30. Energy spectra of protons with energies greater than 15 MeV for slow π^- absorption on heavy emulsion nuclei. Calculated values are for 1 MeV π^- on Ru^{100}. Solid lines: calculated spectrum for medium nonuniform nuclear configuration; long-dash—short-dash lines: calculated spectrum for small uniform configuration; dotted lines: experimental results of Azimov (see Ref. 24). The units of the ordinate are arbitrary.

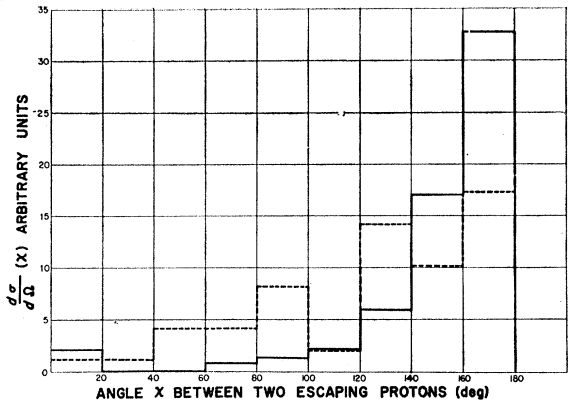

FIG. 31. Angular distribution of two-prong stars as a function of the angle between them. Prongs resulting from 50 MeV π^+ absorption on C. Solid lines: calculated values; dashed lines: experimental values of Laberrigue *et al.* [J. Laberrigue, M. P. Baladine, and S. J. Otivinovski, J. Phys. Radium **21**, 54 (1960)].

The interval associated with the former represents the smallest statistical deviation to be expected from any calculated quantity presented here. The error limits are those for the standard 68% confidence interval.

No other limits are given because it does not seem that they are very meaningful. In the first place most of the distributions for any of the calculated average values are skew symmetric, unless a prohibitive number of histories are used to calculate each average value. In the second place, the standard deviation of the distribution of average values is not known, but must be estimated from one calculated average value (this estimate is based on the assumption that the distribution of average values is normal). And in the third place, the standard error limits cannot be interpreted as a bracket of the true mean value but only implies that the chances that the true mean value lies within the limits are 68%, or that the true mean value will be bracketed by roughly two out of every three such calculated limits.

A fair estimate of the reproducibility of the calculated histograms is to draw an imaginary smooth curve through the histograms and note the deviations from this curve. The true mean value should be within 25% of all of the other calculated values.

TABLE X. Comparison of charge exchange to absorption cross-section ratios.

Energy (MeV)	Ratio of charge exchange to absorption cross section	
	Present calculation	Blinov *et al.*[a]
77	0.39	0.11
136	0.47	0.12
224	0.51	0.24
283	0.57	0.26

[a] See Ref. 29.

CONCLUSIONS

With but one exception, the calculations seem to be capable of reproducing most of the experimental data reasonably well for incident nucleons. This holds for the energy range from about 50 to 350 MeV on all but the lightest elements ($A<12$). The exception is the cascade particle energy spectrum in the forward direction ($\leq 20°$). The existence of a high-energy peak is correctly predicted but the location of the peak is approximately 20 MeV too high.

On the other hand, the best that can be said for reactions involving incident pions in the same energy range is that the gross features of the reactions should be predicted reasonably well. The results for pions break down more rapidly than those for nucleons when detailed information is required. This might be caused by the very large $\pi^+ + p$ resonance in the middle of the energy range under test, which may make the assumption of complete incoherency for pion-nucleon collisions within the nucleus invalid.

In regard to the nuclear configuration, it appears that the bulk of the effect in going from a uniform density distribution to a nonuniform distribution (diffuse nuclear edge) comes from the increased nuclear dimen-

sions. The shape of the distribution yields second-order effects. These effects are largest for the heaviest nuclei.

The accurate predictions of cross sections of the type (p,pn) appear to be beyond the limits of a combined cascade and evaporation code using this model.

There are a few experiments which would be pertinent to some of the discrepancies observed here. One would be a check on the symmetry of the fast-particle multiplicities when fairly heavy elements are bombarded by neutrons and protons of about the same energy. Another would be a careful measurement of the pion-nucleus charge-exchange cross section for a few energies and targets. A few others would be measurements of the spectrum, the angular distribution, and the multiplicities of cascade nucleons emitted for nonelastic scattering of pions or nuclei. There is very little of this type of data and it would assist in determining the causes for some of the discrepancies in pion-nucleus reactions.

The calculation could be improved by including refraction effects at the nuclear surface and by allowing pion absorption to take place on other clusters besides the two-particle ones used here.

AVAILABILITY OF THE CALCULATION AND ITS RESULTS

The following information has been included in this paper rather than elsewhere[31] to comply with the recommendations of the editors.

The calculation is being prepared for release to interested users. It should operate on any IBM-7090 using the standard IBM monitor system. The bulk of the code is written in FAP. Some of the subroutines are written in FORTRAN.

In addition, a large number of cases have already been run.[32] These include incident neutrons and protons with energies ranging from 25 to 400 MeV on ten elements from carbon to uranium. The output includes the angular excitation energy, and momentum distributions of the residual nucleus, the angular and energy spectra of the cascade particles, their multiplicities, and the energy spectra and multiplicities of the evaporation particles (up to alpha particles) along with the radiochemical cross section. Similar cases will be run for incident π mesons.

With a minor change in the code, information can be generated from which the angular momentum remaining in the nucleus at the completion of the cascade can be calculated.

ACKNOWLEDGMENTS

The author would like to state his sincerest appreciation for the help received from Dr. C. D. Zerby who suggested the problem and who took time to discuss any aspect of it whenever help was needed. Some of the preliminary work was done by Professor R. B. Curtis who also made himself available for help and discussion and his assistance is gratefully acknowledged. Many thanks are also due Dr. T. A. Welton for helping to bring this phase of the work to completion, and Professor R. I. Present for his kind advice while reviewing the work.

[31] As an ORNL memo, for example.

[32] There is considerable output for each case. Detailed information pertaining to the type and form of the output which is being made available can be obtained from the author at ORNL, P. O. Box X, Oak Ridge, Tennessee.